CLUSTER-STAFF search coil magnetometer calibration - comparisons with FGM

Patrick Robert, Nicole Cornilleau-Wehrlin, Rodrigue Piberne, Y. de Conchy, C. Lacombe, V. Bouzid, B. Grison, Dominique Alison, Patrick Canu

Geosci. Instrum. Method. Data Syst., 3, 153–177, 2014
www.geosci-instrum-method-data-syst.net/3/153/2014/
doi:10.5194/gi-3-153-2014

Geoscientific Instrumentation Methods and Data Systems
Open Access

CLUSTER–STAFF search coil magnetometer calibration – comparisons with FGM

P. Robert[1], **N. Cornilleau-Wehrlin**[1,2], **R. Piberne**[1], **Y. de Conchy**[2], **C. Lacombe**[2], **V. Bouzid**[1], **B. Grison**[3], **D. Alison**[1], **and P. Canu**[1]

[1]Laboratoire de Physique des Plasmas, CNRS, Palaiseau, France
[2]LESIA-Observatoire de Paris, CNRS, Meudon, France
[3]Institute of Atmospheric Physics, Prague, Czech Republic

Correspondence to: P. Robert (patrick.robert@lpp.polytechnique.fr)

Received: 31 May 2013 – Published in Geosci. Instrum. Method. Data Syst. Discuss.: 12 December 2013
Revised: 18 June 2014 – Accepted: 26 June 2014 – Published: 1 September 2014

Abstract. The main part of the Cluster Spatio-Temporal Analysis of Field Fluctuations (STAFF) experiment consists of triaxial search coils allowing the measurements of the three magnetic components of the waves from 0.1 Hz up to 4 kHz. Two sets of data are produced, one by a module to filter and transmit the corresponding waveform up to either 10 or 180 Hz (STAFF-SC), and the second by the onboard Spectrum Analyser (STAFF-SA) to compute the elements of the spectral matrix for five components of the waves, $3 \times B$ and $2 \times E$ (from the EFW experiment), in the frequency range 8 Hz to 4 kHz.

In order to understand the way the output signals of the search coils are calibrated, the transfer functions of the different parts of the instrument are described as well as the way to transform telemetry data into physical units across various coordinate systems from the spinning sensors to a fixed and known frame. The instrument sensitivity is discussed. Cross-calibration inside STAFF (SC and SA) is presented. Results of cross-calibration between the STAFF search coils and the Cluster Fluxgate Magnetometer (FGM) data are discussed. It is shown that these cross-calibrations lead to an agreement between both data sets at low frequency within a 2 % error. By means of statistics done over 10 yr, it is shown that the functionalities and characteristics of both instruments have not changed during this period.

1 Introduction

Data calibration of spectra and waveforms issued from a search coil magnetometer is not a new problem. Among previous space physics missions using search coil magnetometers, let us mention GEOS-1 and GEOS-2 as the first ESA spacecraft dedicated to the study of waves and particles in the magnetosphere (Knott, 1975; Jones, 1977). The GEOS wave consortium (S300 experiment) comprised a tri-axis search coil magnetometer built by the predecessors of the spatial team of the Laboratoire de Physique des Plasmas (LPP). The technology used in CLUSTER–STAFF experiments has been substantially upgraded since this epoch, but the principle remains the same: how to calibrate magnetic waveforms issued from a search coil rotating across a high ambient DC field, knowing that the transfer function varies with the frequency? This kind of problem has been solved in this epoch for time–frequency studies (Robert et al., 1978, 1979). Nevertheless, since the creation of the CLUSTER Active Archive (Perry et al., 2005), the need to have a continuously calibrated waveform became essential, and a dedicated method, detailed in this paper, was deployed.

To calibrate a set of search coil data is one thing, to be sure that the calibration is right is another thing. It is true for the calibration of any instrument, but particularly important for search coil calibration where the solution is not unique. In fact, it depends on calibration parameters, themselves depending of the frequency band of the signal (see Sect. 6.4). Using the amplitude of the spin tone measured in the spin plane by the search coil, it is possible to compute the two DC

field components in this plane, and so compare them with a fluxgate magnetometer instrument. This was done in the GEOS epoch, where the agreement found was ∼ 4 % in magnitude and ∼ 4° in direction (Robert, 1979b).

As the CLUSTER data are archived and will be used a long time after the lifetimes of the instrument and the corresponding PI and engineers, it was about time to do this work now to get the best possible calibration and to do necessary checks of cross-calibration. Special care has therefore been devoted to the calibration and cross-calibration of the magnetic wave measurements before launch on the ground, then onboard during the commissioning phase, and throughout the mission. A special effort to compare STAFF-SC data with the FGM onboard flux gate magnetometer data (Balogh et al., 1997, 2001) has been undertaken from the beginning of the mission until now. This was encouraged by the Cluster Active Archive (CAA) activities and particularly by the organisation of regular cross-calibration meetings. The present paper, after a short reminder of the STAFF experiment (Sect. 2), presents the instrument transfer functions determined on the ground, followed by the in-flight verification (Sect. 3). A comparison of the sensitivity of the instrument both on the ground and in space is then discussed (Sect. 4). The transformation of the raw data that are acquired in a spinning system (Cluster spacecraft are spin stabilised) into a fixed physically meaningful reference frame needs the series of successive coordinate transformations described in Sect. 5. The conversion of telemetry data into physical units, that is to say the calibration process itself, is then presented for the waveform data (Sect. 6) and for the Spectrum Analyser data (Sect. 7). The continuity of spectral values as well as the similarity in the wave characterisation between the two STAFF experiments are presented in Sect. 8. Section 9 is devoted to the comparison between STAFF and FGM data and to a discussion of the obtained results, followed by the conclusion.

2 Instrument description

STAFF is one of the five experiments of the Wave Experiment Consortium (WEC); see Pedersen et al. (1997). The optimisation of the analysis of the five components of the electromagnetic waves is among the objectives of the WEC. The STAFF experiment comprises a boom-mounted three-axis search coil magnetometer, a preamplifier and an electronics box that houses the two complementary data-analysis packages: the digital Spectrum Analyser, and an onboard waveform unit. The experiment is briefly described below, with some emphasis on elements of interest for further wave characteristic determination and the comparison between the four spacecraft. For a detailed description of the experiment, see Cornilleau-Wehrlin et al. (1997, 2003). The search coils are mounted at the extremity of a radial boom to avoid interferences from the spacecraft. Figure 1 gives a schematic

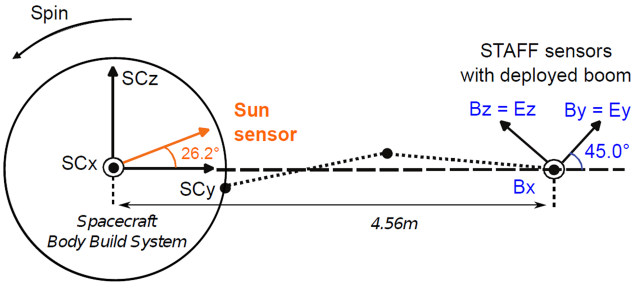

Figure 1. Position of STAFF search coil antennas on the Cluster spacecraft, with respect to the spacecraft and EFW antennas.

of the position of the STAFF antennas with respect to the spacecraft body axis.

The frequency range of the search coil measurements is 0.1 Hz to 4 kHz. The signals go to the preamplifiers, which incorporate a first-order high-pass filter at 0.3 Hz in order to diminish the spin signal. The three output signals then enter the waveform unit, where the analogue waveform signal is sent to different Cluster experiments. First, inside the waveform unit, it is filtered and digitised before being sent to DWP, the Digital Wave-Processing experiment (Woolliscroft et al., 1997) interfacing between wave experiments and the spacecraft. Second, it is sent to the STAFF Spectrum Analyser (STAFF-SA) and to other experiments (see the STAFF block diagram in Fig. 2). These are the Electron Drift Instrument (EDI) (Paschmann et al., 1997), the Wideband (WBD) Plasma Wave (Gurnett et al., 1997) and the Electric Field and Wave experiment (EFW) (Gustafsson et al., 1997). The internal memory of EFW permits, among different possibilities, to get small snapshots of the five-component waveform up to 4 kHz.

The magnetic waveform unit comprises low-pass filters of the seventh order, at either 10 or 180 Hz, selected by telecommand in accordance with the telemetry rate, giving a 42 db attenuation per octave. The sampling rates are 25 and 450 Hz respectively. The output signals are digitised in a real 16-bit analogue-to-digital converter. The 96 dB dynamic range allowed by the 16-bit digitalisation permits the analysis of simultaneously natural waves of a few 10^{-5} nT $Hz^{-1/2}$ and the large signal induced by the rotation of the spacecraft in the environmental DC field, up to some 2000 nT at 0.25 Hz. With such a dynamic range we can get accurate measurements, even at the inversion of the DC magnetic field, e.g. at the magnetopause crossing. The experiment had been designed for its initial orbit, for which the perigee was at a radial distance of 4 Earth radii from the Earth's centre. During the prolongation of the Cluster mission, due to mechanical laws, the perigee has decreased a lot, and there are periods around the perigee where the waveform does saturate. While the data are useless for these periods, this has not induced a degradation of the experiment's capabilities. Owing to telemetry limitations, a reduction in the dynamic data range from 16 to

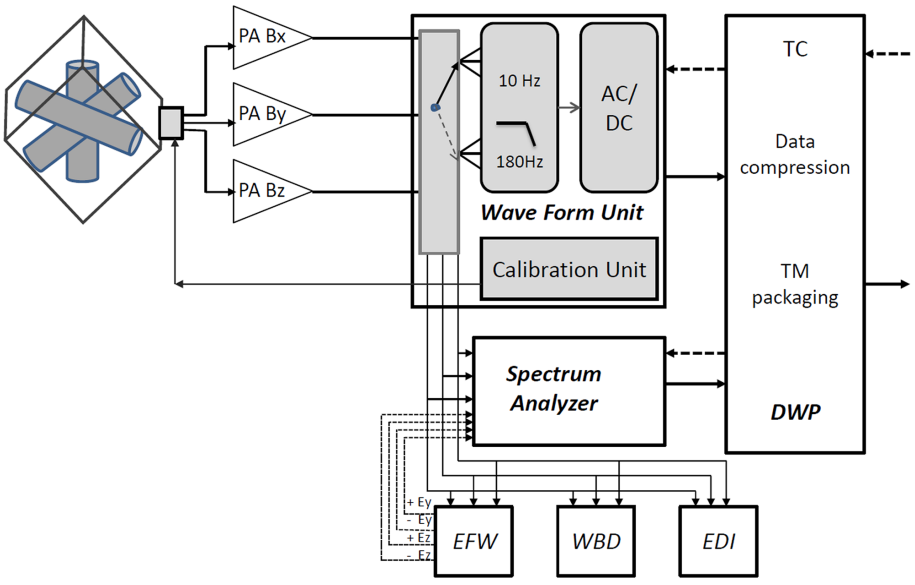

Figure 2. Block diagram of the STAFF experiment and its links to other Cluster experiments.

12 bits is performed inside DWP. The principle is to transmit the full 16-bit word at the beginning of each telemetry packet, and later the difference between the successive samples coded on 12 bits, in such a way that the dynamics of the experiment is preserved even at boundary crossings. Conservative back-up solutions can be selected by telecommand, being either a cruder compression, or having no compression at all. The back-up compression is used during three hours around the perigee, where the spin signal can be above some 200 nT, and at high telemetry rates where the waveform is acquired up to 180 Hz. The three modes have been tested successfully during the commissioning phase.

At higher frequencies for which the telemetry does not permit one to get the waveform, the onboard Spectrum Analyser is part of the STAFF experiment. In addition to the three search coil output signals, the Spectrum Analyser receives the signals from the four electric field probes of the EFW experiment. These are used to form a pair of orthogonal electric field dipole sensors. All five inputs ($2 \times E + 3 \times B$) are used to compute in real time the 5×5 Hermitian cross-spectral matrix at 27 frequencies distributed logarithmically in the frequency range 8 Hz to 4 kHz. The components in the spin plane are despun onboard. All channels are sampled simultaneously, and the integration time for each channel is the same as the overall instrument time resolution, which can be commanded to values between 125 ms and 4 s. The five auto-spectral power estimates are obtained with a dynamic range of approximately 100 dB and an average amplitude resolution of 0.38 dB. The ten cross-spectral power estimates are normalised to give the coherence. The precision of the phase depends upon the magnitude of the coherence: for a signal with magnitude in the highest bin, it is approximately 5° close to 0, 180, and $\pm 90°$, increasing to about 10° midway between these angles.

The STAFF waveform box also houses an onboard calibration unit that permits one to detect a potential failure of a part of the experiment and to recalculate the transfer function in case of any variation in the experiment response, which is crucial for the comparison between the four spacecraft. The calibration sequence, run once every orbit, consists in sending successively a white noise and fixed-frequency sine waves (~ 7 and 100 Hz), the intensity of which is diminished step by step. The calibration signals are sent at the input of the search coil through the feedback wiring (Fig. 7 of Cornileau-Wehrlin et al., 1997).

3 STAFF experiment transfer functions

3.1 Initial transfer functions

The magnetic sensors together with their associated preamplifiers were first calibrated on the ground. There is a special facility at a quiet site in the Forest of Orléans which is located at the Chambon-la-Forêt Observatory. The calibration facility was built by previous members of the laboratory in the 1960s. The facility consists of a set of three 1 m diameter Helmholtz loops orthogonally mounted to generate a magnetic field. At the centre is a table on which the sensors to be calibrated are put. This table can move around a central axis and is carefully graduated. This facility is also equipped with big loops that were intended to compensate for the Earth's magnetic field. In fact this is not used, as for search coils we are only concerned with rapid (faster than 10 s) variations in the magnetic field. Free space field and stimuli are used, to get respectively the instrument sensitivity and transfer

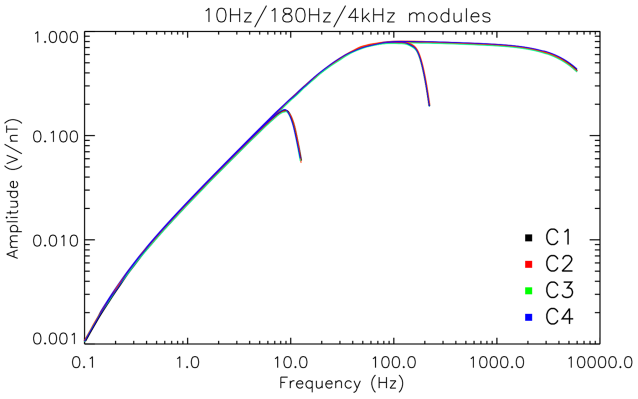

Figure 3. Amplitude of the transfer functions as a function of the frequency, at the output of the preamplifier for the whole frequency range 0.1 Hz–4 kHz, and at the output of the 180 Hz and the 10 Hz filters respectively, for the Bx component. Data for the four spacecraft are overplotted.

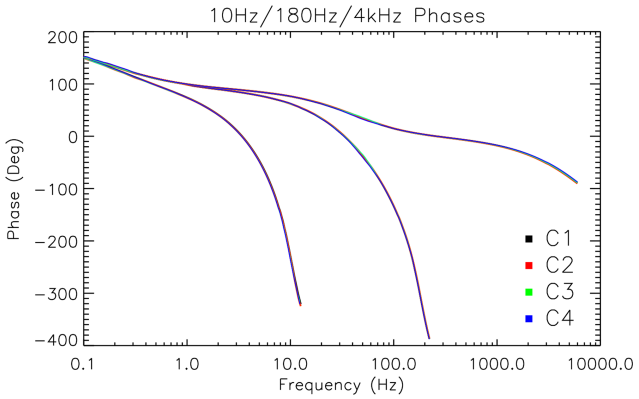

Figure 4. Phase of the transfer functions in degrees as a function of the frequency, at the output of the preamplifier for the whole frequency range 0.1 Hz–4 kHz, and at the output of the 180 Hz filter and the 10 Hz filter respectively, for the Bx component. Data for the four spacecraft are overplotted.

function. We measured there the transfer functions of the antennas and of their respectively associated preamplifiers. The 10 and 180 Hz filter transfer functions have been established in the laboratory, not at the Chambon-la-Forêt Observatory. The deduced combined transfer functions at the output of the antennas and preamplifiers, and at the output of two-range high-pass filters 10 and 180 Hz, are plotted in Figs. 3 and 4. The transfer functions of the four spacecraft are overplotted, for one component, Bx, and do not show significant differences (see Sect. 3.3 below).

Another quantity has been measured in Chambon-la-Forêt: the angle between the mechanical axis of the search coil antennas and the magnetic axis. This is obtained by rotating the antennas on the table and knowing the mechanical axis, and by looking at the antenna response at each angle, we determine the antenna diagram. The angles are small, and the axis can be assumed to be aligned, within an error smaller than 0.3°. The orthogonality of the three axes has also been verified. By the way, from the spin signal seen on the Bz axis (parallel to the spin axis), it has been shown that the angle between the spacecraft spin axis and the Z antennas is of the order of 0.5°. As it has been decided not to take into account this small misalignment, it has been also decided to neglect the very small non-orthogonality of the sensors. Note that $\sin(0.5°) = 0.0087$, which is close to 1 %. As we will see in Sect. 9, 1 % is also the best agreement found between STAFF and FGM, with all sources of errors. Another work could take into account these small errors, but it should be done at once for STAFF and FGM. It could be done in the future.

3.2 Corrections applied to the initial transfer functions

While measurements during the commissioning phase showed that the sensitivity and transfer functions were as expected from ground measurements (see Fig. 2 of Cornilleau-Wehrlin et al., 2003), it appeared during scientific operation that we observed a systematic underestimation of SC1 measurements of about 10 % at low frequencies, in particular at the spacecraft spin frequency. Moreover, comparisons of STAFF waveform data with FGM data evidenced another 10 % underestimation. The reasons for these differences have been studied and explained, leading to a correction of the transfer functions. It is those corrected transfer functions that are given in Figs. 3 and 4. Let us explain the different issues. First we look at the 10 % difference between SC1 and the others. Going back to records of measurements in Chambon-la-Forêt, we found that the current loop axis we used for SC1 was not the same as for the other spacecraft. In addition, the big loops aimed at compensating for the DC Earth magnetic field, which was aligned with the current loop axis used for SC1 antennas, but which was not used for the other spacecraft search coils, disturbed the magnetic field by means of an induced magnetic field opposite to the one produced by the current loop even at very low frequencies. This explained the differences between SC1 and the others. Second, looking very carefully at each of the three current loops, we then found that their structures were no longer perfect plane circles. All this has been verified by means of a reference search coil (that has been tested by different Helmholtz coil facilities and compared with predicted measurements). From this a corrective transfer function has been established:

$$\mathrm{FT\_CORR} = 1.1 \times \frac{\left(1 + j\frac{f}{\mathrm{fch}}\right)}{\left(1 + j\frac{f}{\mathrm{fcb}}\right)},$$

with fch = 85 Hz and fcb = 102 Hz.

The transfer functions of SC 2, 3 and 4 are corrected by this formula. The corrected transfer function of SC 1 is computed by averaging the other three complex transfer functions. The new transfer functions thus obtained have

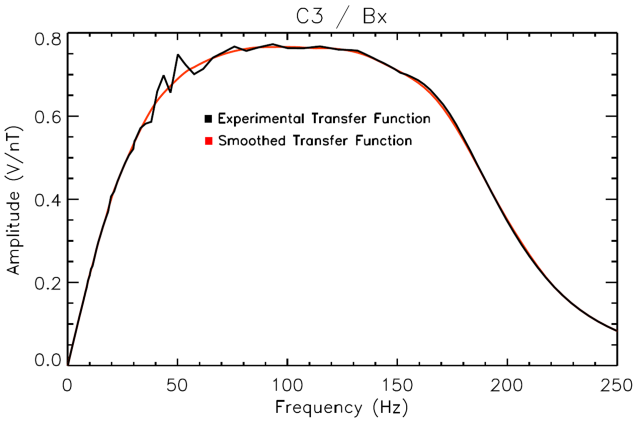

Figure 5. Example of a smoothed transfer function, here the Bx component for SC3, at the output of the 180 Hz filter. The influence of power lines at 50 Hz is clear; this has been smoothed.

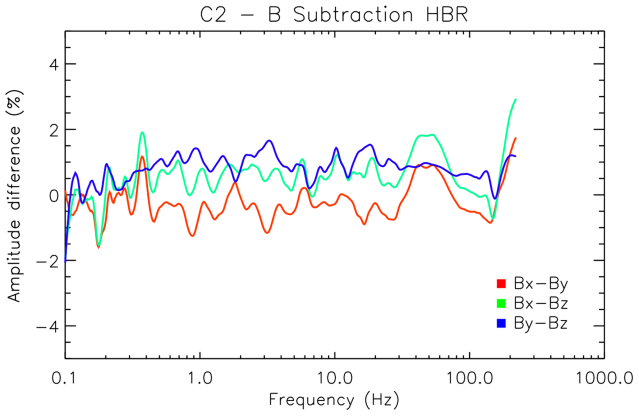

Figure 6. Example for SC2 of the normalised difference in the answer in amplitude of the three components of the magnetic waveform data on the spacecraft.

been applied to STAFF data and compared again with FGM data, as will be shown later on in this paper, giving satisfactory results. It was then estimated that we had found the error sources, and that we could not go further. This comparison seems to show that the facility loops had already undergone the deformation at the time of Cluster STAFF search coil calibration, in 1999, observed some years previously. Since then, a new set of lops, as circular, planar and orthogonal as possible, has been installed at Chambon la Forêt Oservatory.

As the site magnetic quietness is not perfect, there remain some variations in the transfer function which were attributed to the environmental electric array, namely at 50 and 150 HZ. This lead to a smoothing of the new transfer function, as can be seen in Fig. 5.

3.3 Similarity of the search coils, between the three components and between the four spacecraft

As the aim of the Cluster mission is to perform three-dimensional measurements, this implies the ability to combine the data of the different spacecraft either to derive quantities as a curl to get e.g. small-scale currents or to apply the so-called K-filtering method (Pinçon and Lefeuvre, 1991) to disentangle possible different waves modes in turbulent spectra, it was a requirement to produce four experiments as similarly as possible (see e.g. Fig. 4 in Cornilleau-Wehrlin et al., 1997). An example is given in Fig. 6 below, where it can be seen that the relative difference in response in amplitude of the transfer function in the frequency range 0.1–180 Hz is less than 2 %. The normalised differences $Bx–By$, $Bx–Bz$ and $By–Bz$ are overplotted in red, green and blue respectively. For other spacecraft and for 10 Hz filter output, the normalised differences have the same order of magnitude. Note that the differences start to increase around 180 Hz, where the low-pass filters start to be efficient.

3.4 In-flight calibration

As mentioned above (Sect. 2), in order to verify the health of the experiment in operation, the in-flight calibration mode is run once per orbit. A systematic check is done as soon as the data arrive in the lab to verify that data remain within given limits. This did not lead to any unexplained alarm. More detailed analysis can be done – and will be done – to analyse how the experiment behaves after 12 yr (or more) of operation, being built for 2 yr. An example of such a check is given in Fig. 7. This is the result of the analysis of the white noise which is sent by the onboard cal-box to the search coils, using the feedback wires of the search coils. In this step of the calibration mode, the strongest signal is sent. After a Fourier transform of the signal, it is averaged in successive frequency bands to facilitate the verification. The power as a function of the frequency reflects the combined transfer functions of the search coils and the 10 Hz filter. In the figure, two data sets are superimposed, one obtained at the beginning of the mission in 2001 and the other recently in 2012, in the same period of the year (same region of the magnetosphere). One can see the stability of the experiment's behaviour with time.

4 STAFF sensitivity

The determination of the instrument's magnetic sensitivity is an important issue in what concerns the validity of the scientific data analysis. As mentioned in the previous section, the instrument's sensitivity is determined on the ground at the quiet site of Chambon-la-Forêt. An example is given in Fig. 8, onto which have been superimposed to the ground-determined sensitivity the results of measurements in space when in a region with no wave activity (lobes of the magnetosphere). The in-flight data are for one spacecraft (SC4) on one day. Data from STAFF-SA and from waveforms in the 10 and 180 Hz bands are overplotted. The

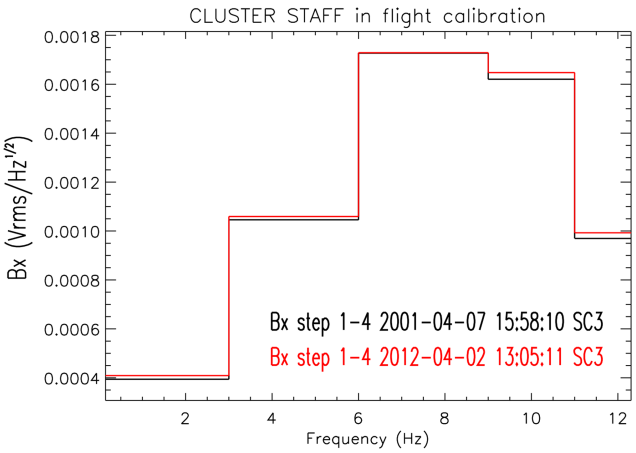

Figure 7. Superimposition of the result of two periods of in-flight calibration in 2001 and 2012. Here a pseudo white noise sent to the search coil antennas is measured at the output of the 10 Hz filter.

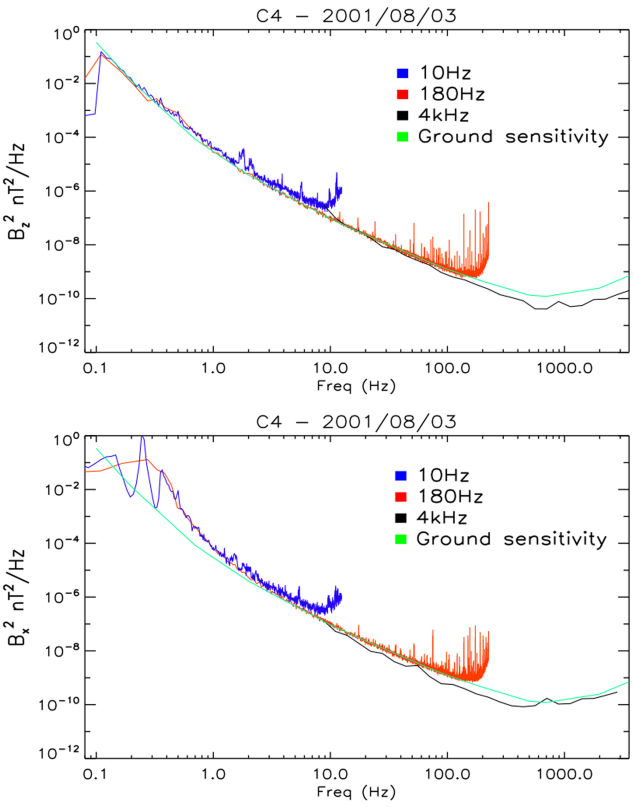

Figure 8. Example of comparison of the sensitivity measured on the ground (green line) at the quiet site of Chambon la Forêt and in flight during a quiet period, for SC4 Bz (top panel) and Bx (bottom panel) components (By is identical to Bx). Outputs of Spectrum Analyser (black line) of 180 Hz filter (red) and 10 Hz filter (blue) are superimposed (see text).

10 and 180 Hz filter data cannot be simultaneous, but are close in time. Bz is plotted on top and Bx at the bottom. One sees that the in-flight STAFF-SC data are as good as on the ground. For STAFF-SA output, the in-flight sensitivity is better than the ground sensitivity; indeed, the in-flight experimental noise is below the ground sensitivity curve. This could be explained by the absence in flight of the 50 Hz power line signal and its harmonics seen on the ground. Nevertheless, a few interferences are seen, at 70, 140 and 280 Hz, internal to STAFF-SA, and at 900 Hz, coming from the DWP clock. When looking at the background noise for the 180 Hz waveform, one sees some thin interference lines, the frequencies of which vary from time to time and from one spacecraft to another. This may limit the sensitivity of the measurements in the higher frequency range. The increase in the noise level at and above 10 Hz (180 Hz) comes from the cut-off frequencies of the filters. Due to the effect of the spin signal (see below), the noise level is higher on Bx than on Bz (parallel to the spin axis) at low frequencies.

Figure 9 intends to show the possible evolution of the noise level with time. The spectra are obtained up to 9 Hz by 10 Hz low-pass filter waveform data, and above 9 Hz, they come from STAFF-SA. The above-mentioned interferences are seen clearly on Bx (and By), mainly on Cluster 3 and Cluster 2. Data are averaged over one hour, taken in quiet periods in the same region for the four periods, in the Earth's lobes. Data for spacecraft 1 to 4 are plotted from top to bottom, with Bx components on the left and the Bz ones on the right. Being similar to Bx, they are not shown. One can notice the rather stable level with time, with nevertheless some increase for the A frequency band of STAFF-SA (8–64 Hz). The higher level at low frequencies ($f < 0.3$ Hz) is due to an effect of the local spin signal (high level of DC magnetic fields).

5 Sensor rotation and coordinate systems

To transform telemetry data into significant physical units, we need to convert the data from the sensor coordinate system into one or another system, and in particular to transform from the spinning system into a fixed one, with respect to the Sun and the Earth, for instance. For the waveform data, all transformations are done on the ground, whereas for STAFF-SA data, part of the transformation is done on board. The following sections are dedicated to defining all intermediate coordinate systems required for this operation. Notice that these definitions can be used for other experiments of the same type, on any other mission.

All transformation matrices are named as A_to_B, where A and B are two different coordinate systems. To convert a vector given in the A system to the same vector expressed in the B system, the following expression is used:

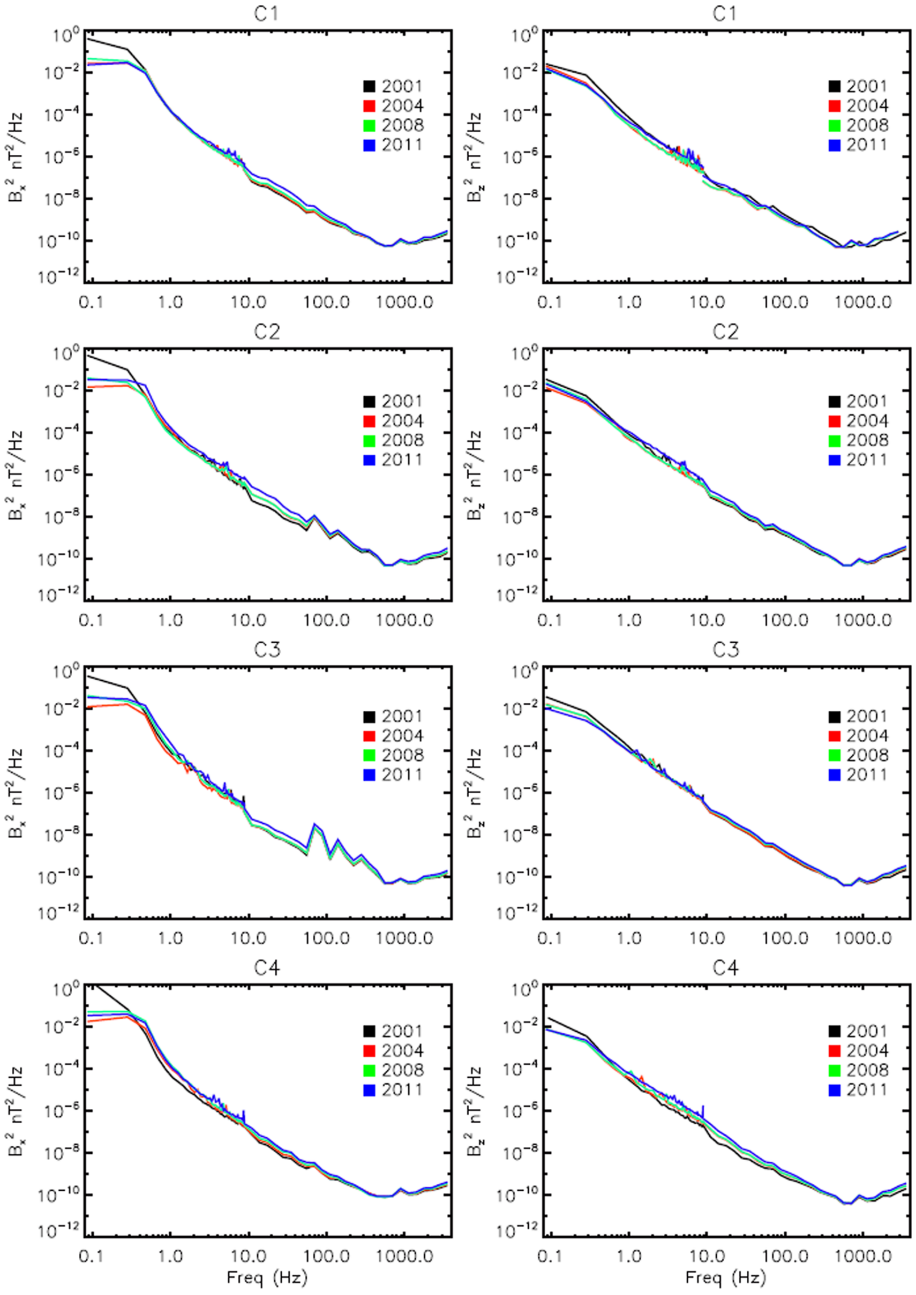

Figure 9. Evolution of the sensitivity with time, for four different years, in the lobes (quiet region) for the four spacecraft and for the Bx and Bz components (By, not shown, is similar to Bx) for both parts of the experiment (waveform up to 9 Hz, Spectrum Analyser above 9 Hz). The chosen time intervals are 3 August 2001 12:00–13:00 UT, 12 August 2004 11:00–12:00 UT, 12 August 2008 19:00–20:00 UT and 19 August 2011 00:10–01:10.

$$\begin{pmatrix} x \\ y \\ z \end{pmatrix}_B = A\_\text{to}\_B \begin{pmatrix} x \\ y \\ z \end{pmatrix}_A .$$

For a general computation of this kind of matrix, see Robert (1993, 2003, 2004).

5.1 The Sensor Coordinate System (SCS)

This is the system where the original signal is measured (see Fig. 1). This system could be a non-perfect orthogonal system (see Sect. 3.1).

5.2 The Orthogonal Sensor System (OSS)

This is a Cartesian orthogonal coordinate system. The original sensor system can be a non-orthogonal system. The first step is to transform the data vector into an orthogonal coordinate system, the Z axis being the reference of the new orthogonal sensor system. The corresponding matrix, called "SCS_to_OSS", close to a unit matrix, is required and must be applied; values are supposed to be constant in time. Nevertheless, for the first time, taking into account the low deviation of the sensor to an orthogonal system for CLUSTER–STAFF ($\sim 0.2°$, see Sect. 3.1), this correction is not applied and the matrix is set to the unity matrix.

$$\text{SCS\_to\_OSS} \cong \begin{pmatrix} 1 & 0 & 0 \\ 0 & 1 & 0 \\ 0 & 0 & 1 \end{pmatrix}$$

5.3 The Data Sensor System (DSS)

The Body Build System (BBS, see next section) is a system fixed to the geometry of the spacecraft, and is used as the spacecraft system reference for all the experiments. Generally, for most of the spacecraft missions, the Z axis is close to the maximum principal inertia axis also called the spin axis (for spin-stabilised spacecraft). Nevertheless, for CLUSTER, this axis has been defined as the X axis (see Fig. 1).

In all our data, the convention taken is that Z is the spin axis. It means that we have an intermediate coordinate system, called the Data Sensor System (DSS), which corresponds to the previous OSS, but where the axes are permuted to make Z close to the spin axis.

With respect to Fig. 1, X_{OSS}, Y_{OSS}, and Z_{OSS} become Y, Z, and X in DSS.

This permutation is obtained by the following matrix:

$$\text{OSS\_to\_DSS} = \begin{pmatrix} 0 & 1 & 0 \\ 0 & 0 & 1 \\ 1 & 0 & 0 \end{pmatrix}.$$

5.4 The Body Build System (BBS)

In the case of CLUSTER, the Z axis of the Data Sensor System is close to the X axis of the BBS, but the misalignment angle is not easy to determine. It is also true for the small angle between this X_{BBS} and the true spin axis (precession and nutation motions). Nevertheless, an estimate of the cumulative angle is made in Sect. 5.5. Here, we neglect this small misalignment and assume that $Z_{\text{DSS}} = X_{\text{BBS}}$. In all cases, two other axes may be rotated by an important angle (see Fig. 1). The corresponding matrix is required, called "DSS_to_BBS"; values are supposed to be constant. Practically, for the STAFF search coils of CLUSTER, this matrix is a rotation matrix of $\alpha = 45°$.

$$\text{DSS\_to\_BBS} = \begin{pmatrix} 0 & 0 & 1 \\ \cos\alpha & -\sin\alpha & 0 \\ \sin\alpha & \cos\alpha & 0 \end{pmatrix}$$

5.5 The Spin Reference System (SRS)

The Spin Reference System has its Z axis parallel to the spin axis. This is a spinning system, rotating at the spin frequency. As mentioned above, there is a small misalignment between the X_{BBS} axis and the Z_{SCS} axis, as there is another slight misalignment between the X_{BBS} axis and the Z_{DSS} axis. It is not easy to separate the two angles, but it is possible to estimate the small angle between the Z_{SCS} axis and the true spin axis which defines Z_{SRS}. This angle θ could be estimated by the measurement of the low spin signal on the Z_{SCS} component.

If $B_{x\text{s}}$, $B_{y\text{s}}$, and $B_{z\text{s}}$ are the amplitudes in nT of the spin sine on the three x, y, and z components of the SCS, this angle is estimated by

$$\tilde{\theta} = \frac{B_{z\text{s}}}{\sqrt{B_{x\text{s}}^2 + B_{y\text{s}}^2 + B_{z\text{s}}^2}}.$$

This angle could be constant, but can also have small variations during operations on the spacecraft (trajectory modifications, etc.). It has been estimated to an average value of $\sim 0.5\,\%$, and, for the first time, has not been taken into account, so the "BBS_to_SRS" matrix is set to

$$\text{BBS\_to\_SRS} \cong \begin{pmatrix} 0 & 1 & 0 \\ 0 & 0 & 1 \\ 1 & 0 & 0 \end{pmatrix}.$$

This is a simple circular permutation.

5.6 The Spin Reference2 (SR2) system

The SR2 system, also called "SSS" for Spacecraft-SUN System, or "DS" for despun, is derived from the SRS by a *despin* operation. The spinning spacecraft is "stopped" just at the time where the X axis is in the plane containing the Z spin axis and the direction of the Sun. The rotation angle required is derived from the Sun pulse, which gives the time where the Sun sensor is in the plane defined by the spin axis and the direction of the Sun. Knowing the position of the Sun sensor onboard the spacecraft (see Fig. 1) and the time of each telemetry point, we can deduce the spin phase angle φ_{s}. This angle, and the corresponding time measurement, is required to build the "SRS_to_SR2" matrix. The terms of this matrix are fast varying with time. f_{s} is the spin frequency given in the auxiliary data. The phase angle φ_{s} is calculated for each time tag of the data thanks to the Sun pulse signal. This gives

$$\text{SRS\_to\_SR2} = \begin{pmatrix} \sin(2\pi f_{\text{s}} t + \varphi_{\text{s}}) & \cos(2\pi f_{\text{s}} t + \varphi_{\text{s}}) & 0 \\ \cos(2\pi f_{\text{s}} t + \varphi_{\text{s}}) & -\sin(2\pi f_{\text{s}} t + \varphi_{\text{s}}) & 0 \\ 0 & 0 & 1 \end{pmatrix}.$$

5.7 The Geocentric Solar Ecliptic (GSE) system

The GSE system is a well-known system, with the Z axis perpendicular to the ecliptic plane, and the X axis toward the

Sun. To do the transformation of the SSS to the GSE, the direction of the spin axis in the GSE system is required. Due to the gyroscopic effect of a spinning spacecraft, the spin axis is approximately constant in an inertial system, and so has a yearly variation in the GSE system, except during spacecraft manoeuvres.

SR2 to GSE transformation is done using the module "tsr2gse" routine of the ROCOTLIB software (see Robert, 1993, 2003, 2004). The Cartesian GSE coordinates of the direction of the spin axis are required as the corresponding time measurement. To transform spin right ascension and the spin declination angle given in the STAFF-SC CAA data in the Geocentric Equatorial Inertial (GEI) system, routine "tgeigse" can be used. These angles are also available in the auxiliary files available at CAA (latitude and longitude angles of the spin axis direction in GSE).

Note that in the GSE system, each component mixes both parallel and perpendicular components with the spin axis. Because sensitivity is strongly different at low frequencies in the parallel and perpendicular components in the SR2 system, it is recommended to filter the data below ~ 0.6 Hz before coordinate transformation. This is done for CAA Complex Spectra products.

5.8 The Inverse SR2 (ISR2) system

This is equivalent to the SR2 system (or SSS), where the Z and Y axes have inverse signs. This system is useful for CLUSTER, where the Z axis of the ISR2 system is close to the Z axis of the GSE system, so ISR2 is a rather good approximation of the GSE system, and does not require spin direction in the GSE system.

$$\text{SR2\_to\_ISR2} = \begin{pmatrix} 1 & 0 & 0 \\ 0 & -1 & 0 \\ 0 & 0 & -1 \end{pmatrix}$$

5.9 Simplification of the cumulative matrix products

The cumulative matrix product requested to transform original data given in SCS coordinates into a fixed coordinate system such as SR2 can be greatly simplified if we neglect all the small misalignment angles mentioned above. By the way, the first mass processing on the STAFF-SC data was to produce a database for the level 1 data (telemetry data) in the DSS, which is delivered to the CAA. The only difference between the DSS and the SCS sensor coordinate is a circular permutation of the components to get the Z axis close to the spin axis, since we assume that the SCS is orthogonal and equal to the OSS (see Sect. 5.3).

So, to transform data expressed in the DSS into the "fixed" SR2, we have to apply the cumulative matrix product:

$$\begin{pmatrix} x \\ y \\ z \end{pmatrix}_{\text{SR2}} = [\text{SRS\_to\_SR2}][\text{BBS\_to\_SRS}][\text{DSS\_to\_BBS}] \begin{pmatrix} x \\ y \\ z \end{pmatrix}_{\text{DSS}}.$$

Assuming all small misalignment angles to be close to zero, we get

$$[\text{BBS\_to\_SRS}][\text{DSS\_to\_BBS}] = \begin{pmatrix} \cos\alpha & -\sin\alpha & 0 \\ \sin\alpha & \cos\alpha & 0 \\ 0 & 0 & 1 \end{pmatrix}.$$

Using the expression "SRS_to_SR2" given in Sect. 5.6, with $\omega_s = 2\pi f_s$ after some calculus we get

$$\begin{pmatrix} x \\ y \\ z \end{pmatrix}_{\text{SR2}} = \begin{pmatrix} \sin(\omega_s t + \varphi_s + \alpha) & \cos(\omega_s t + \varphi_s + \alpha) & 0 \\ \cos(\omega_s t + \varphi_s + \alpha) & -\sin(\omega_s t + \varphi_s + \alpha) & 0 \\ 0 & 0 & 1 \end{pmatrix} \begin{pmatrix} x \\ y \\ z \end{pmatrix}_{\text{DSS}}.$$

By neglecting all the small misalignment angles, the transformation from the Data Sensor System to the fixed SR2 system is simply reduced to a rotation in the spin plane of the fast varying angle $\psi = (\omega_s t + \varphi_s + \alpha)$.

This simplification is used for CLUSTER–STAFF calibration, but cannot be used for spacecraft or rockets having precession or nutation, or a non-constant direction of the spin axis. In this case, the full computation must be done.

6 STAFF-SC calibration method

6.1 Spectrum calibration in sensor frame

The STAFF-SC experiment is a waveform unit which delivers magnetic waveform $x(t)_{\text{Volt}}$ in the SCS sensor reference frame. The transfer function being frequency dependent but not proportional, all components of this signal at various frequencies must be corrected both in amplitude and phase, so the signal delivered by the search coil is

$$x(t)_{\text{Volt}} = \int_{-\text{fs}/2}^{+\text{fs}/2} X(f)_{\text{nT}} \alpha(f) e^{2i\pi f t} \mathrm{d}f, \quad (1)$$

where $X(f)$ is the spectrum of the true ambient signal, in nT, $\alpha(f)$ is the complex transfer function of the sensor in V nT^{-1}, and fs/2 is the upper detectable frequency in Hz.

For the first time, let us consider the calibration of a single spectrum.

After digital processing, fs being then the sampling frequency, Eq. (1) becomes

$$x_{k(\text{Volt})} = \sum_{-N/2}^{N/2} X_n \alpha_n e^{2i\pi nk}. \quad (2)$$

X_n is the Fourier transform of the real signal x_k, in nT, to be estimated. The spectral resolution is $\delta f = f_s/N$.

So, to retrieve the original spectra (in nT), a simple Fourier transform is required:

$$X_n = \frac{1}{\alpha_n} \frac{1}{N} \sum_{-N/2}^{N/2} x_k e^{-2i\pi nk}. \quad (3)$$

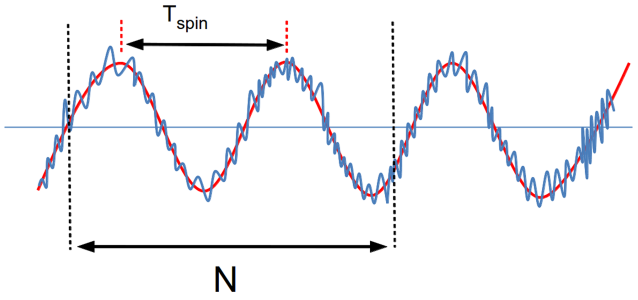

Figure 10. Spin tone superimposed onto rapid variations of the magnetic field that the search coils intend to measure.

Figure 11. Trapeze and round trapeze used as weighting functions.

This is the theory. In practice, the original x_k signal is formed by a large sine signal at spin frequency fspin (~ 0.25 Hz), due to the rotation of the sensors into a large DC field (~ 100 nT), and the fluctuations (a few nT) are superimposed, so the amplitude of the "useful" frequency range is ~ 100 times less intense than in the DC field (spin signal at ~ 0.25 Hz, see Fig. 10). Furthermore, a Fourier transform assumes a periodic signal of period N, and thus introduces large discontinuities on the edges of the window which generate meaningless high-frequency components (see Robert et al., 1978, Robert, 1979a).

Thus, the first step is to remove this large sine signal with dedicated software which computes the amplitude and phase of the sine for a given spin frequency and removes it. Note that this measurement of amplitude and phase on the two Bx and Bz DSS spinning components allows us to compute the two components in the spin plane of the DC field, by applying the complex coefficient of the transfer function at the spin frequency, taking into account the phase angle given by the Sun pulse time to convert results into a non-spinning frame system (see later). Then, to avoid discontinuities on the edge of the window, the second step is to apply a weighting function on the signal after centering on zero. The weighting function must preserve the shape of the signal, but must also ensure that the weighted signal is periodic, so that its edges fall to zero. By experience, the choice of a very long trapezoid works well, as shown in Fig. 11.

So, the estimate of the original spectrum (in nT) is computed by

$$\tilde{X}_n = \frac{1}{\alpha_n}\frac{1}{N}\sum_{-N/2}^{N/2} x_k W_k e^{-2i\pi nk}.$$

Before computing the estimate of the calibrated waveform $\tilde{x}_{k(nT)}$, we now have to study the successive coordinate systems used to convert the signal recorded by the sensors into a useful coordinate system.

6.2 Computing calibrated waveforms in the SR2 system

From Eq. (3) we can estimate the calibrated waveform in the SCS by an inverse FFT, as

$$\tilde{x}_{k(nT)} = \sum_{-N/2}^{N/2} \tilde{X}_n e^{2i\pi nk}.$$

Afterward, the calibrated waveform in the SR2 system is computed by applying the successive coordinate system matrix defined in Sects. 5.1 to 5.6; practically, for CLUSTER–STAFF, we use the simplified equation given in Sect. 5.9, and we get

$$\begin{pmatrix}\tilde{x}_k\\ \tilde{y}_k\\ \tilde{z}_k\end{pmatrix}_{\mathrm{SR2}} = \begin{pmatrix}\sin(\omega_s t_k+\varphi_s+\alpha) & \cos(\omega_s t_k+\varphi_s+\alpha) & 0\\ \cos(\omega_s t_k+\varphi_s+\alpha) & -\sin(\omega_s t_k+\varphi_s+\alpha) & 0\\ 0 & 0 & 1\end{pmatrix}\begin{pmatrix}\tilde{x}_k\\ \tilde{y}_k\\ \tilde{z}_k\end{pmatrix}_{\mathrm{DSS}}.$$

One result is that the SCS and the DSS differ only by a circular permutation (see Sects. 5.2 and 5.3).

6.3 Computing the calibrated spectrum in the SR2 system

The previous waveform being calibrated and expressed in the SR2 system, the complex spectra is simply given by the FFT of this calibrated waveform, as

$$\tilde{X}_n = \frac{1}{N}\sum_{-N/2}^{N/2} x_k W_k e^{-2i\pi nk}.$$

The weighting function can be chosen freely. For CLUSTER–STAFF CAA products, we chose a trapeze function as described in Fig. 11. For other applications, an alternative could be a "rounded trapeze", by replacing the edges with a $\sin^2$ function rather than a line. The same operation is of course done for $\tilde{Y}_n$ and $\tilde{Z}_n$.

6.3.1 Window effect

Due to the weighting function, the previous calibrated waveform is significant only around the centre of the window. To

enlarge this part, we generally use a weighting function, the shape of which is a trapeze or a rounded trapeze represented in Fig. 11. We can see that only $\sim 7/8$ of the waveform is significant.

In normal use, the length of the window is about a few spin periods. At least one spin period is required to estimate the amplitude and phase of the sine, and two or three spin periods allow a best estimate. Beyond a few spin periods, the DC field could change significantly, and the spin tone estimate will be less accurate. A good compromise is between one and four spin periods to estimate properly the DC field and to remove spin tone.

6.3.2 Summary of the various steps done during spectrum calibration

Calibration of the telemetry data is done in successive steps, described below. At this level, the calibration is done on successive data windows to obtain the calibrated spectra as described above.

Get waveform in volts

Telemetry data are given in integer values (called TM counts) within a [0, 65 535] interval corresponding to a volt range of [−5, +5 V]. The value of 65 535 comes from the used sample words of 16 bits in length. This step does the conversion simply as

$$x\,(t_n)_{\mathrm{Volt}} = \left[x\,(t_n)_{\mathrm{TM}} \times 10/65\,535\right] - 5.$$

Selecting the time length of the windows determines the Δt. Δf is one resolution of each spectrum.

This step is named "Calibration step #1: Volts, spinning sensor system, with DC field".

Cleaning raw waveforms

This step consists in removing the high-amplitude signal at spin frequency due to the SC rotation into a high DC field. Indeed, the wave useful signal is very low (a few nT) compared with the high spin tone (a few nT, up to $\sim$ 5–600 nT). Even if the transfer function coefficient in amplitude is small at the spin frequency, the spin tone in volts remains too high to do a correct fast Fourier transform (see Robert, 1979a).

This step is named "Calibration step #2: Volts, spinning sensor system, without DC field".

The independent calibration of the spin tone, both in amplitude and phase, on the two Bx and By components allows the determination of the two components in the spin plane, which can be compared with the same components measured by the FGM experiment.

Calibration of each component within a given window

For the first time the signal is centered, and then a light trapezoidal windowing is applied to reduce edge effects before applying the FFT. Next, in the frequency domain, for each frequency, the complex spectrum is divided by the complex transfer function to get a calibration in amplitude and phase. Since the transfer function is close to zero for frequencies close to zero, a cut-off frequency is applied, generally fixed at 0.1 Hz. Lastly, an inverse Fourier transform is performed to return in the time domain and to get a calibrated waveform in the given window, always in the Sensor Spinning System.

This step is named "Calibration step #3: nTesla, spinning sensor system, without DC field".

Get the calibrated waveform in the fixed SR2 system

By applying the appropriate matrix given in Sect. 6, which requires spin phase computation, one gets the calibrated waveform in the SR2 system.

This step is named "Calibration step #4: nTesla, fixed SR2 system, without DC field".

Add DC field values on X and Y

This is an optional step which allows comparison with FGM data, because one obtains, for the two X and Y components in the spin plane, both the DC field and the fluctuation.

This step is named "Calibration step #5: nTesla, fixed SR2 system, with xy DC field".

Get the calibrated waveform in the GSE system or others

This is an optional step. From step 4, waveforms can easily be converted in the GSE system or other geocentric systems (GSM, MAG, GEO ...) by using the ROCOTLIB software (see Robert, 1993, 2003, 2004).

Remark: this method provides a calibrated waveform *which is only significant in the central part of the window*, and produces discontinuities at the edges of each window, so this method cannot be used to produce continuously calibrated waveforms (see Robert, 1979a, 2009). The method used to produce continuously calibrated waveforms is described in the next section.

Nevertheless, this method can be used to produce the estimate of the calibrated spectrum $\tilde{X}^{\mathrm{SR2}}_{n(\mathrm{nT})}$ in the SR2 system (see Sect. 6.3) by applying a simple Fourier transform. The main advantage is the low CPU time consumption.

6.4 Waveform continuous calibration method

6.4.1 Method chosen for CLUSTER

To obtain a continuous waveform, we have to repeat the previous operation by overlapping successive windows and keeping the central points, as illustrated in Fig. 12. The calibration is done on a window of Nkern telemetry (TM) points, which determines the frequency resolution of the intermediate calibrated spectrum, that is the accuracy of the calibration. The calibration window is then shifted by Nshift points.

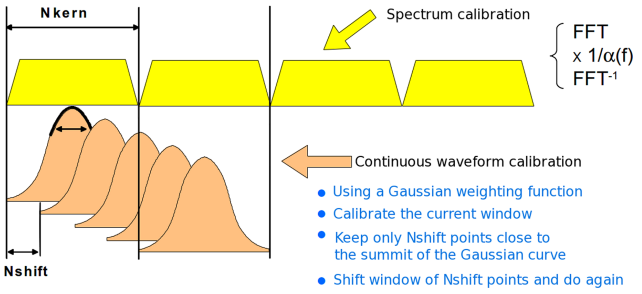

Figure 12. Illustration of the continuous calibration method (bottom) as compared with spectrum calibration.

The Nkern number must be optimised in order to

– Do a correct despin: the window duration must be long enough to have a good estimate of the spin tone, but not too long, because the amplitude (and phase) of the spin tone varies with time; the DC field could change in both direction and amplitude. A good compromise is between 2 and ~ 10 spin periods. One period is the minimum to run the despin algorithm.

– Have a high enough frequency resolution: the window duration must be long enough to get a significant sampling of the transfer function and to get a good accurate calibration.

The number Nshift must be optimised in order to

– Be the shortest possible, for instance two points corresponding to the summit of the weighting function in the window.

– Reduce CPU time by increasing Nshift, but quality will be reduced too. If the weighting function is not constant during the Nshift point centered on the window, a parasite line appears on the spectrograms at fsr/Nshift frequency (fsr being the sampling rate).

Tests show that the best result is obtained by using a Gaussian weighting function, and by shifting the windows from one to the next one by two points, saving each time the two central points at the summit of the Gaussian.

For the CLUSTER–STAFF-SC CWF CAA production, the chosen values for the Nkern and Nshift parameters are given in Table 1. These values have been chosen to process a calibration which works whatever the amplitude and the time variation of the DC field, under normal conditions. This is important, because we can see that by the choice of the calibration parameters, *the solution for the calibration data is not unique*. For very particular conditions, these parameters can be adjusted to get the best quality of the calibration. For instance, if low frequencies are not interesting, it is preferable to filter the data above twice the spin frequency, to avoid undesirable spin effects. The length of the calibration window

Table 1. Parameters chosen for the routine production at CAA for the continuous calibration of the waveform as a function of the sample frequency.

	Sample freq. (Hz)	NKern	Window duration (s)	Spin period (s)	Nshift
NBR	25	1024	40.95	~ 10	2
HBR	450	4096	9.10	~ 2.3	2

also plays a role in the calibration, depending on whether the covered period is stationary or not. In a general way, a long window leads to a more accurate calibration, but is time consuming, and enlarges the data gap. However, a long window could also lead to a non-perfect cleaning of the large sine signal due to the DC field, especially if it is fast varying. In any case, the best compromise must be sought in relation to the nature of the data (stationary waves or magnetopause crossing can require different calibration parameters). This is why we keep available in the Cluster Archive the level 1 waveform (uncalibrated). It is the expertise of the experimenter that will lead to better results.

6.4.2 Other calibration methods

The previous method, which is a deconvolution in the frequency domain, can be summarised by

$$x_{k(\mathrm{nT})} = \mathrm{FFT}^{-1}\left\{\frac{1}{\alpha_n}\mathrm{FFT}\left(x_{k(\mathrm{Volt})}w_k\right)/\right\}.$$

More recently, the THEMIS mission has also included search coils (Roux et al., 2008), and for the data processing we used the deconvolution in the time domain (Le Contel et al., 2008), which can be summarised by

$$x_{k(\mathrm{nT})} = \left(x_{k(\mathrm{Volt})}w_k\right) \times A_k,$$

where "$\times$" is the convolution operator and A_k the impulse function of $\frac{1}{\alpha_n}$, i.e. $\mathrm{FFT}^{-1}\left\{\frac{1}{\alpha_n}\right\}$.

From Plancherel's theorem, notice that the two expressions are equivalent:

$$\begin{cases} x(t_k) \times A(t_k) \Leftrightarrow & X(f_n)\cdot\alpha(f_n) \\ x(t_k)\cdot w(t_k) \Leftrightarrow & X(f_n)\times W(f_n) \end{cases}.$$

We find again in this method the concept of Nkern and Nshift, with the same meaning, as the weighting function, and the need of "cleaning" the waveform by removing the spin tone before any other processing.

Comparison of the two methods has been done by applying the two different software packages to the same data set, and concludes with a good agreement. Details of these comparisons will be done in another paper. Note that the calibration software used for CLUSTER is written in Fortran90,

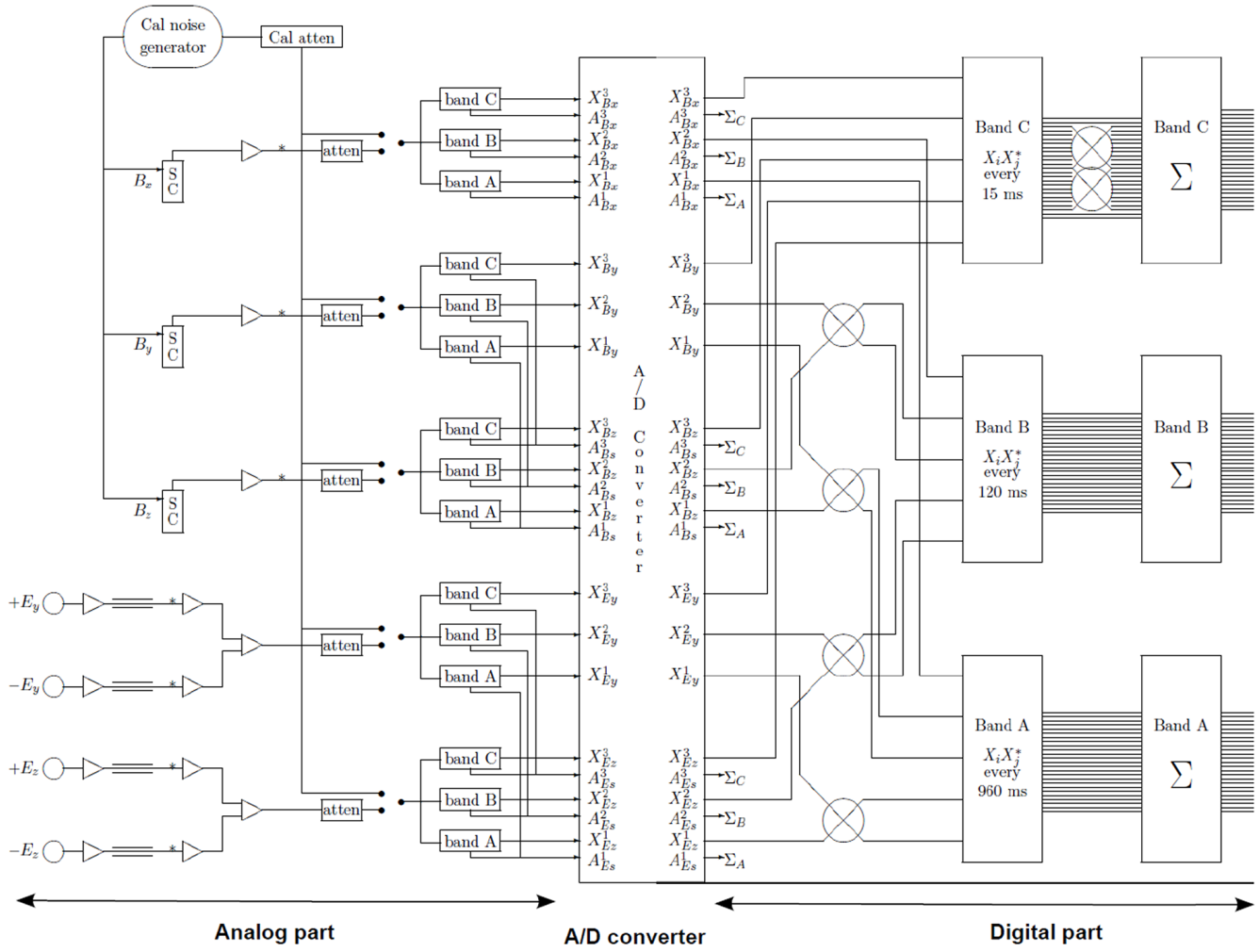

Figure 13. The different parts of the STAFF Spectrum Analyser instrument (STAFF-SA). From left to right: analogue part, A/D converter, digital part.

while the calibration software used for THEMIS is written in IDL. In this last case, the convolution operation has been done by the built-in "CONVOL" IDL function, which is very efficient. So, the good agreement of the two results is a proof of the validity of these two programs, which is very important for validating archive databases.

7 STAFF-SA Spectrum Analyser

STAFF-SA has 5 input channels connected to 5 sensors: 3 magnetic and 2 electric. An overview of the instrument is given in Fig. 13. It makes estimations of the auto- and cross-spectral power density at 27 frequencies, arranged into 3 bands, A, B, and C, which have their own automatic gain control.

7.1 Onboard calculations

The separation into three bands is performed by the analogue part of the receiver. The digital part performs the despin for the spin-plane components and makes a filtering in nine narrower frequency bands. It then calculates the cross-spectral matrix of the five components in amplitude and in phase. The AGC are fixed during the time of an analysis, time controlled by telecommand. The different steps of the onboard calculation can be seen in Fig. 14, and for more details on the onboard calculation, see Sect. 4.3 of Cornilleau-Wehrlin et al. (1997).

In order to calculate the cross-spectral matrix, the components that are in the spin plane are despun:

$$B_u = B_y \cos(m) + B_z \sin(m)$$
$$B_v = B_z \cos(m) - B_y \sin(m),$$

where m is the instantaneous angular position of the spacecraft as derived from the onboard Sun reference pulse (SRP),

and u and v are the fixed coordinates corresponding to the position of the STAFF search coil (SCS) antennas at the time of the Sun pulse (i.e. when the SRP sees the Sun, see Fig. 1). The angle between this reference frame and the SR2 reference frame is then $45–26.2 = 18.8°$.

7.2 Routine on-ground calibration

The calibration model that is applied on the ground to the raw spectral matrix data is a combination of mathematical algorithms and tables of coefficients (S(AGC), D(AGC), $\tilde{S}$ (Freq), $\tilde{D}$ (Freq)) used by these algorithms. The set of coefficients comes from measurements performed in the laboratory, including the inverse transfer function of the sensors, STAFF search coils and EFW antennas. The spin-plane receivers are strapped together in pairs with common AGC outputs. The calibration model will treat the sum and the difference of both the receivers. It is convenient to assume that the frequency-dependent and AGC-dependent variations of the analogue transfer function can be separated.

Functions S and D take account of the variation in the AGC level, assumed to be the same for all frequencies within any given band. The parameters S characterise the analogue receivers; the mean spectral noise density in the overall preconverter passband of analogue receiver m is a function of the corresponding AGC output A.

Functions $\tilde{S}$ and $\tilde{D}$ allow for the variation with frequency within each digital input channel. The parameters $\tilde{S}$ characterise the bandpass of the digital spectrum analyser and also the variation with frequency of the analogue receivers. They allow independent auto- and cross-spectral estimates to be obtained in both amplitude and phase at each of the nine frequencies f.

To calculate $\tilde{S}$ and $\tilde{D}$, we have chosen a reference noise level corresponding to AGC = 80 (AGC = 0 to 255). To this ideal calibration we had foreseen to apply a small correction in two different cases: first if the spin is not nominal, i.e. is different from 4 s, this parameter being routinely provided by the spacecraft auxiliary data; second if the spin-plane receivers are not identical. In this later case, the correction parameters have been identified during ground tests of the instrument before launch (Harvey et al., 2004).

To calculate the spectral matrix, we use an iterative numerical method, with a convergence test to stop the calculation. Note that we have assumed the variation of autocorrelations with the AGC level to be the same for all frequencies, within any given band; this is not entirely true for some frequencies, and it can explain some small anomalies. The last operation is to transform the data that are in a non-standard fixed reference frame into SR2. For the components that are in the SC spin plane, a rotation of delta $\varphi = -18.8°$ has to be applied, as well as a BBS-to-SRS rotation matrix to have Bz parallel to the spin axis (see Sect. 5).

This overall treatment of STAFF-SA data gives the complete complex spectral matrix (SM), the diagonal coefficients of the matrix being the power spectral density (PSD) for the five components, in physical units. These PSD diagonal coefficients are kept at a better time resolution than the overall SM. To obtain from the spectral matrix the polarisation and propagation parameters, one can use the PRASSADCO program that has been specifically developed for use by Cluster STAFF-SA (Santolik, 2003), as can be seen in the following section.

8 STAFF-SC/STAFF-SA continuity and other cross-checks

Once the transfer function is calculated, one of the first checks is to compare the results of the data analysis by the two STAFF sub-experiments. Both continuity in the spectra and similarity in the wave characterisation results have been checked.

8.1 Power spectra

For this purpose we have used a special mode of operation which allows the maximisation of the frequency overlap between the two experiments, between 8 and 180 Hz. Examples of different kinds of wave data are given below in Fig. 15. Two kinds of wave fluctuations are shown, for two different spacecraft. Only the Bx and Bz components are shown. Whereas the overlap and continuity are rather good, one can be aware of some effect on STAFF-SA at lower frequencies, as reported in the CLUSTER–STAFF CAA calibration report (Robert et al., 2012).

8.2 Wave characteristic determination

It is important to determine the characteristics of measured waves, which can be done by means of the three magnetic orthogonal sensors. The parameters that can be obtained at one point of measurement are, in particular, wave planarity, ellipticity, sense of polarisation, and propagation angle with respect to the main magnetic field.

These quantities are obtained on the ground for the waveform data up to either 10 or 180 Hz, depending on the telemetry mode, whereas the coefficients of the complex spectral matrix are calculated onboard by the STAFF-SA for the frequency range 8 Hz–4 kHz. Figure 16 gives an example of such an analysis performed by data coming from both the waveform (left panel) and from SA (right panel), observed by Cluster 1 close to the magnetopause on 26 March 2007. The colour scale is the same for both data set analyses, but the frequency resolution is different: linear for waveform data and log for SA. The top panel shows the dynamic spectra. Different polarisation and propagation parameters are then plotted in the time–frequency plane for amplitudes greater than a minimum level only (for PSD larger than 10^{-6} nT^2 Hz^{-1}). These parameters are the ellipticy of the emission, the propagation angle theta (k, B), and the

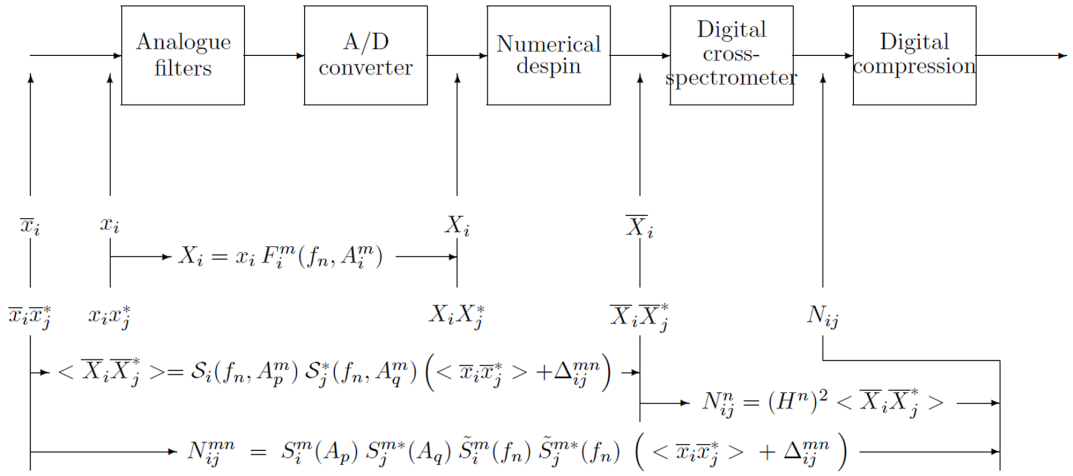

Figure 14. Relationships between the different signals in STAFF-SA.

azimuth angle ($\phi = 0$ indicates the spacecraft Sun direction projected in the plane perpendicular to B). The three polarisation parameters are computed through the singular value decomposition method (Santolik et al., 2003) using the PRASSADCO tool (Santolik, 2003).

The common frequency band between STAFF-SA and STAFF-SC is about 60–225 Hz. The main emission observed during that time interval is detected between 07:22:45 and 07:23:30 UT around 50 Hz, and up to more than 200 Hz in the middle of the time interval. One can remark that the polarisation and propagation parameters calculated from the two data sets give the same results, in the limit of their respective frequency and time resolutions. During this event, the magnetic emissions were clearly right-hand polarised: the theta angle was most of the time less than 45°, and the phi angle displays a nice rotation (from −90 to −180, 180 then to 90°). The similar values of the different parameters obtained from both parts of the experiment, together with physically "reasonable" results, give some confidence in the validity of the data processing performed. This kind of test was performed at the beginning of the mission in order to find an error in the rotation matrix, which has been solved since.

9 STAFF-SC/FGM comparisons

9.1 Interest of such a study

The possibility of recovering two DC magnetic field components by the search coil experiment is particularly useful, because it allows a comparison with the result of the Fluxgate Magnetometer experiment. It has already been done for the GEOS mission (see Jones, 1977); here the agreement found was ∼ 4 % in magnitude and ∼ 4° in direction (Robert, 1979b).

For CLUSTER, the two STAFF and FGM experiments have run successfully since the beginning of the mission. In the framework of the CAA cross-calibration meeting, it was obvious to look after a comparison of the result of the two instruments in their common frequency range. This is not only useful for data validation, but this also permits the clarification of the respective roles of the two instruments.

So, during all calibration meetings, from 2006 until now, the STAFF-FGM comparisons were day by day in progress. Thanks to this kind of comparison, we realised that the transfer function of the search coils was underestimated (Robert, 2nd Cross Calibration Workshop, 2006). After investigation, it was shown that the shape of the calibration device (Helmholtz coils) was slowly distorted with time (see Sect. 3.2 and Robert, 14th Cross Calibration Workshop, 2011). New calibration tables were used, and the STAFF-FGM agreement improved.

9.2 Data origin

FGM data are issued from CAA, in "full" resolution mode, in the GSE system. They are converted into the SR2 system to compare the spin plane components with STAFF-SC data.

Search coil data are calibrated following the process described in Sect. 6.4, in normal bit rate mode (NBR) sampled at 25 Hz mode, and of course in the SR2 system. Step 5, "nTesla, fixed SR2 system, with xy DC field", is used.

9.3 Direct waveform comparison

9.3.1 A typical event studied on various scales

The following results have been shown in different cross-calibration meetings. The 24 February 2001 case is interesting, because we can look at it on various timescales. Figure 17 shows a waveform comparison between 21:00 and 22:00 UT. The $B_\perp$ component is computed from B_{xs} and B_{ys} components in the spin plane as

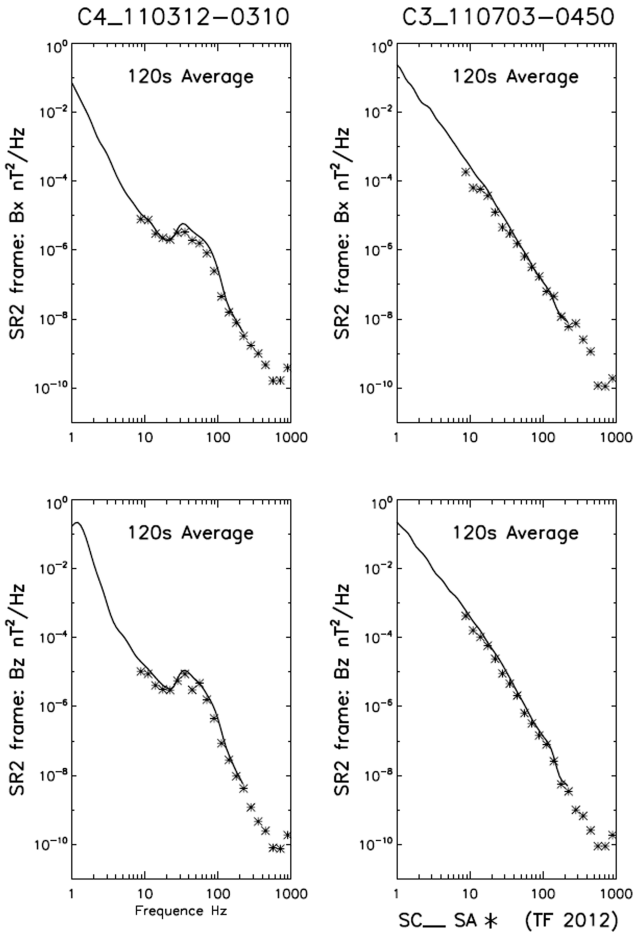

Figure 15. Examples of a comparison between a wavelet spectrum of the waveform data (black line) and a STAFF-SA spectrum (cross). A special operation mode has been used to maximise the overlap between the two experiments, between 8 and 180 Hz. Here are the Bz and Bx components for two different events (left and right sides respectively).

$$B_\perp = \sqrt{B_{xs}^2 + B_{ys}^2},$$

while the direction or phase φ is computed from

$$\sin\varphi = B_{ys}/B_\perp$$
$$\cos\varphi = B_{xs}/B_\perp.$$

On the $B_\perp$ component, at a first glance, the agreement is good, with

$$\frac{\Delta B_\perp}{B_\perp} = \frac{\left(B_\perp^{\mathrm{STA}} - B_\perp^{\mathrm{FGM}}\right)}{\left(B_\perp^{\mathrm{STA}} + B_\perp^{\mathrm{FGM}}\right)/2} \sim 4\%,$$

while the phase angle difference is

$$\Delta\varphi = \left(\varphi^{\mathrm{STA}} - \varphi^{\mathrm{FGM}}\right) \sim 5^\circ.$$

After re-sampling the data to obtain the same sample rate on the two data sets, we can compute the mean difference point to point, and the result is much better:

$$\frac{\Delta B_\perp}{B_\perp} = 0.77\%$$
$$\sigma B_\perp = 0.84\%.$$

If we zoom in on the narrow spike between 21:56 and 21:58 UT (Fig. 18), we can see that the agreement is also good on a short timescale ~ 2 mn. We find as previously that

$$\frac{\Delta B_\perp}{B_\perp} < 1\%$$
$$\Delta\varphi \cong 3^\circ.$$

9.3.2 Statistic over 10 yr on spin plane DC field

Figure 19 shows statistics performed over 10 yr of STAFF-FGM DC field comparisons. The 58 events altogether have been chosen, under four various conditions each year:

- low DC field, low ULF activity,
- low DC field, high ULF activity,
- high DC field, low ULF activity,
- high DC field, high ULF activity.

Figure 19a shows the relative difference $\Delta B_\perp/B_\perp$ in %, where we can see that this difference is roughly constant for each spacecraft during the 10 yr studied.

Figure 19b shows the standard deviation of $\Delta B_\perp/B_\perp$, which is between 0.5 and 5 %, except for one point at 12 %, but which corresponds to a very low $B_\perp$, so $\Delta B_\perp/B_\perp$ become relatively high, taking into account the accuracy of the measurement.

Figure 19c shows the amplitude of the $B_\perp$ DC field for each event, from a few nT to 500 nT.

Lastly, panel d gives the phase difference of the $B_\perp$ component in the SR2 system.

Concerning the relative stability of $\Delta B_\perp/B_\perp$, we can see that it is independent of the magnitude of the DC field, whatever the level of ULF activity. Furthermore, for each spacecraft, this difference remains constant all over the ten-year study. This is an important result, because it shows that the transfer function remains constant from the beginning of the mission until 10 yr after. This result could be confirmed by a dedicated study of the onboard calibration signals.

Another important result is the difference from one spacecraft to another: in fact, the best result seems be obtained for SC1, where the transfer function has been obtained by the averaging of the three others (SC2, SC3 and SC4). This result is thus directly directed by the estimate of the transfer function on the ground, and gives an estimate of their accuracy (see Sect. 3). The choice has been made to keep each of the 3×4 transfer functions slightly different, but, as these tables should theoretically all be identical, another choice could have been to set all tables to the SC1 average table. This could be done in a future work.

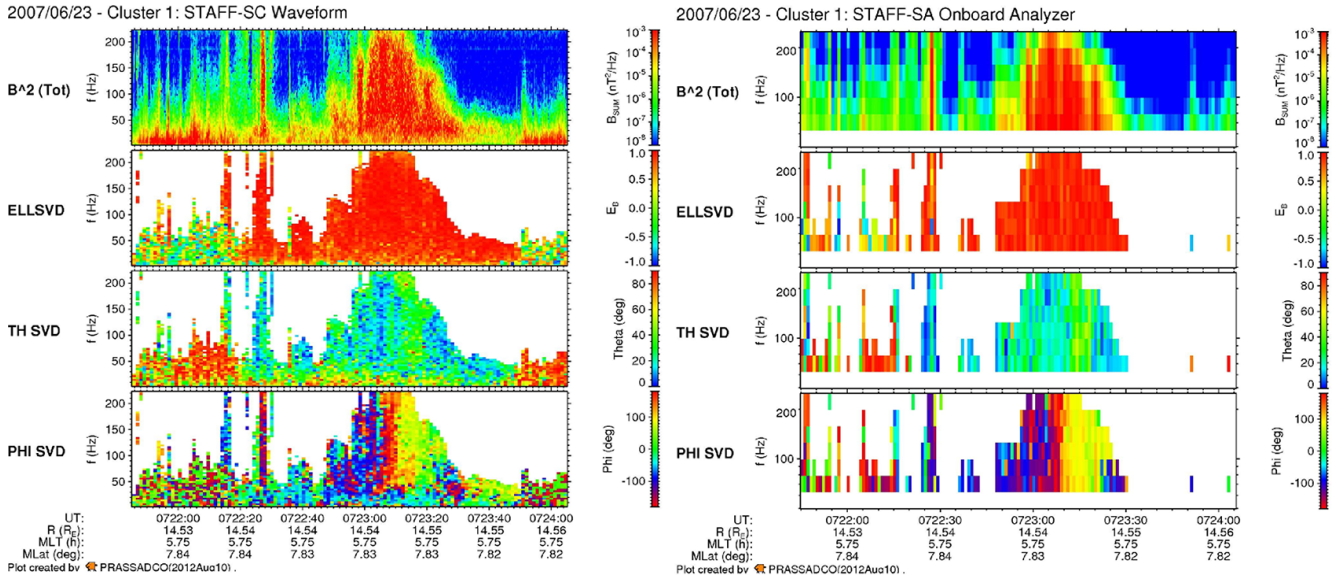

Figure 16. For each instrument (Waveform data – STAFF SC, and Spectrum Analyser – STAFF SA), the same polarisation and propagation characteristic quantities are plotted in a frequency–time diagram: from top to bottom, the total magnetic PSD (power spectral densities), the ellipticy, the propagation angle $\theta(k, B)$ and the azimuth angle (ϕ). To highlight the polarisation of the intense emissions, parameters are plotted only for PSD values, above a threshold. Note that the frequency scale is linear for STAFF-SC and log for STAFF-SA.

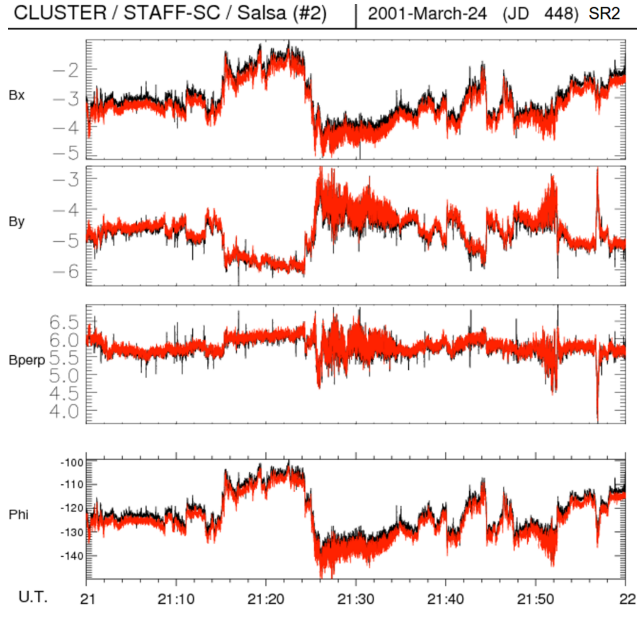

Figure 17. Direct waveform comparison on a large scale (15th Cross-Calibration Workshop, 17–19 April 2012). Black: STAFF, red: FGM.

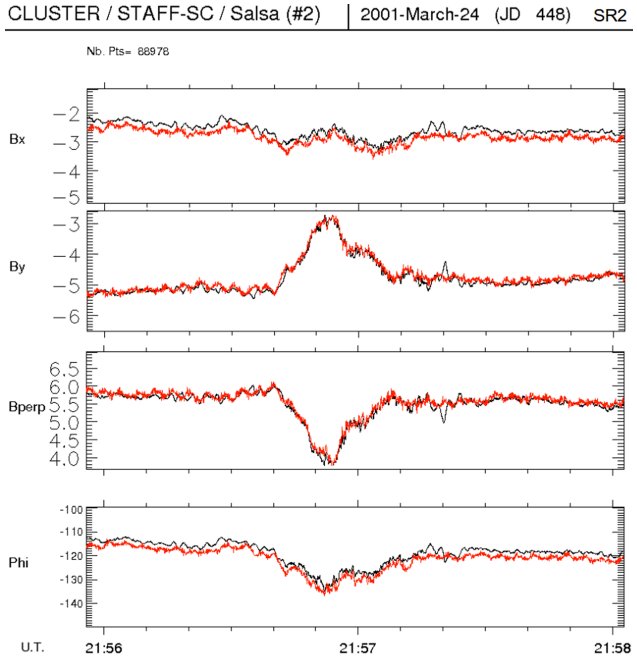

Figure 18. Zoom on 2 min of data around the spike seen at 21:57 UT of Fig. 17. (15th Cross-Calibration Workshop, 17–19 April 2012). Black: STAFF, red: FGM.

Concerning the direction, most of the time this $\Delta\varphi$ difference is between 2 and 4°. Nevertheless, for some cases, this difference changes in sign, and is between -2 and -4°. This change has not been explained up to now.

9.3.3 Comparison at 1 Hz

Figure 20 shows an event with an almost monochromatic wave at low frequency ($\sim$ 1 Hz) superimposed onto a low DC

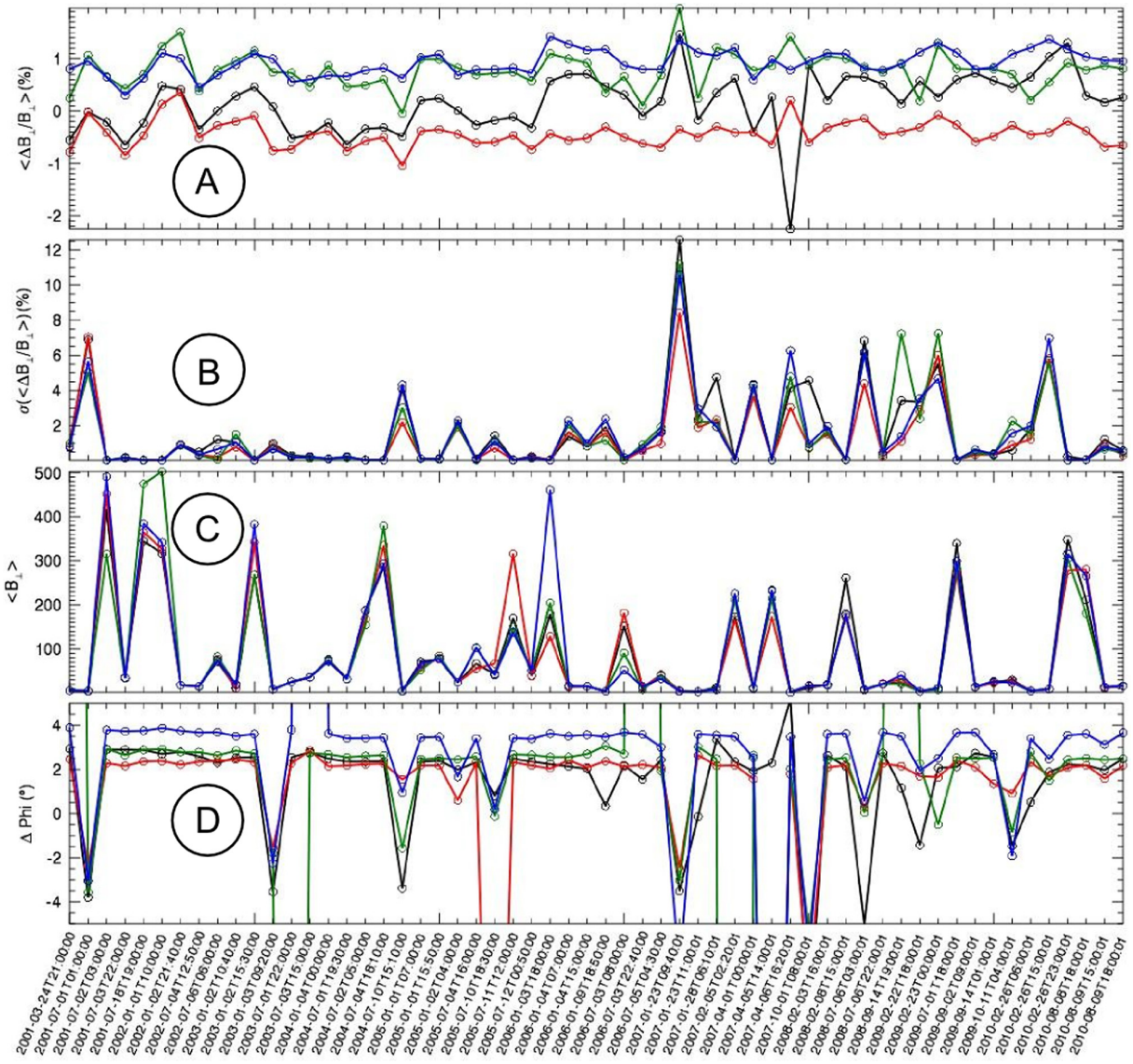

Figure 19. Statistics over 10 yr of STAFF-FGM spin plane DC field comparison for the four spacecraft (black, red, green, and blue for spacecraft 1, 2, 3, and 4, respectively).

variation. In the left part, one can see a constant difference of $\sim 1\,\%$ in the $B_\perp$ component, as expected, and a phase difference of $\sim 4°$. The zoom (in the right part) still shows the same agreement on the DC part, both in amplitude and phase. To see a more precise comparison for the component at 1 Hz, we shift the FGM data of 3.3 nT (1.1 %) to have a better superimposition of the two curves (Fig. 21). The result is rather satisfying, a good fit being found at a first glance, but a spectral analysis is required to get a best estimate of the difference (see Sect. 9.4.1).

9.3.4 Comparison at 6 Hz

The following example corresponds to another almost monochromatic wave at ~ 6 Hz, always superimposed onto a low DC variation (Fig. 22). The wave occurs at $\sim 09{:}39$ UT on By. Agreement on DC fields remains the same ($\Delta B/B < 1\,\%$, $\Delta\phi \sim 3°$).

By zooming on the wave (Fig. 23), we can identify a ~ 6 Hz wave whose amplitude and phase seem to be in good agreement, but as previously, a spectral analysis is required to get more details (see Sect. 9.4.2).

9.4 Spectrum comparison

9.4.1 STAFF-SC/FGM sensitivity

Figure 24 shows a spectrum of STAFF and FGM done during a very quiet period, which means that these two curves can be considered to be the sensitivity of the two instruments. The

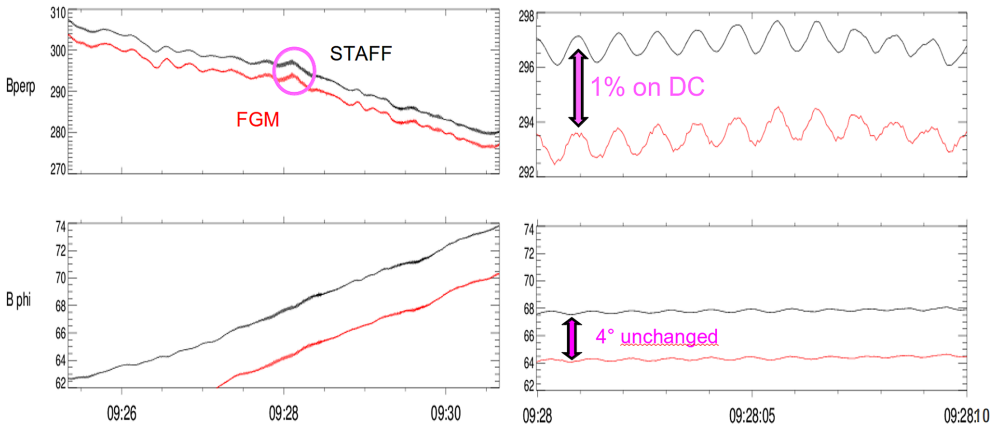

Figure 20. Wave comparison at 1 Hz (CLUSTER–Tango (#4), 23 September 2001).

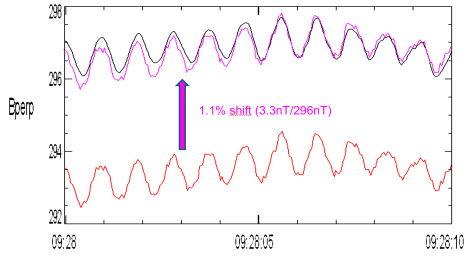

Figure 21. Wave at 1 Hz, STAFF-FGM superimposed.

two curves cross at ∼ 0.7 Hz, that is to say that at this frequency the two instruments have the same sensitivity. Below 0.7 Hz, FGM is not only more sensitive, but of course gives the three components of the DC field contrary to STAFF. Above 0.7 Hz, the search coils are more sensitive and can detect events of smaller magnitude. This leads to the choice of the one experiment rather than the other, according to whether you look at DC or at waves, and for waves, to which frequency range you want to focus on. In fact, the two experiments are quite complementary.

9.4.2 1 Hz event

Figure 25 shows the FGM and STAFF spectra corresponding to the waveform event of Fig. 20. The strong peak at 1 Hz spreads from 0.5 to 1.5 Hz, and the agreement between the two instruments is very good, even for the second peak at ∼ 2.5 Hz. To quantify the exact difference, a dedicated study should be done, requiring filtering of the high frequencies, spike removal and Shannon interpolation for the SATFF-FGM resampling. The noise above 3 Hz is higher for FGM, as expected; nevertheless, it is above the sensitivity shown in Fig. 24.

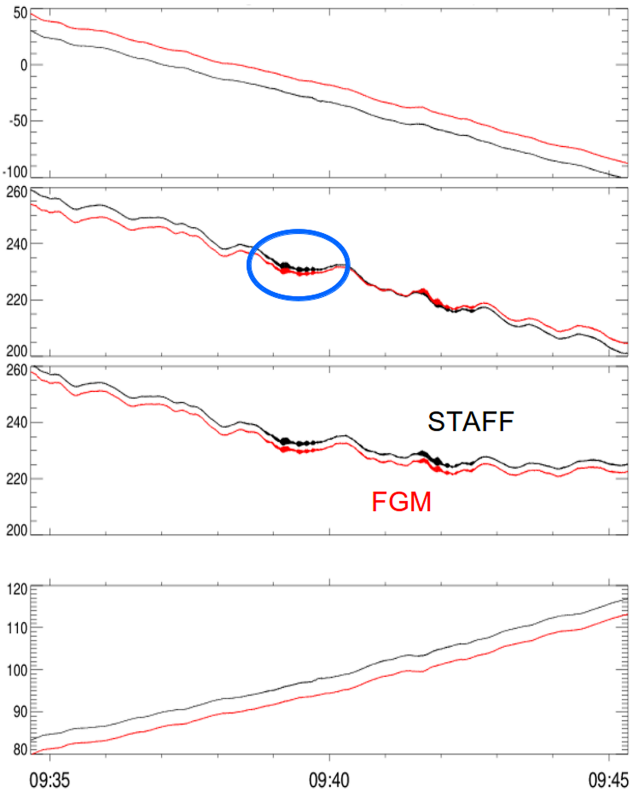

Figure 22. Wave comparison at 6 Hz (CLUSTER–Tango (#4), 23 September 2001. 14th CAA cross-calibration meeting, York, 5–7 October 2011).

9.4.3 6 Hz event

Figure 26 shows the spectra corresponding to the waveform event at 6 Hz of Figs. 22 and 23. As above, the strong peak at 6 Hz spreads from ∼ 4.5 to 6.5 Hz, and shows very good agreement between STAFF and FGM. Nevertheless, the second peak at ∼ 7.75 Hz is not recorded by FGM, its sensitivity not being sufficient at this frequency. On the other hand, a

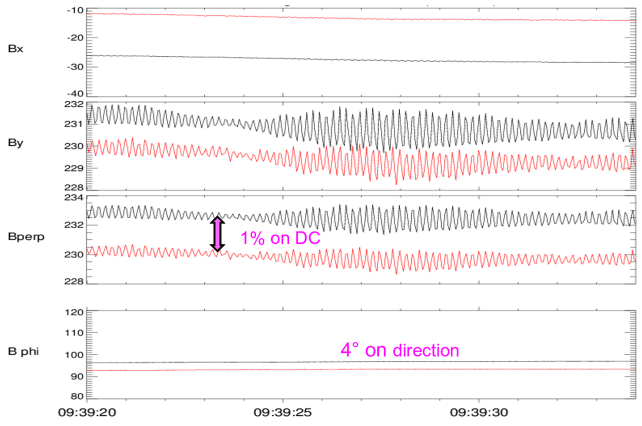

Figure 23. Zoom on wave comparison.

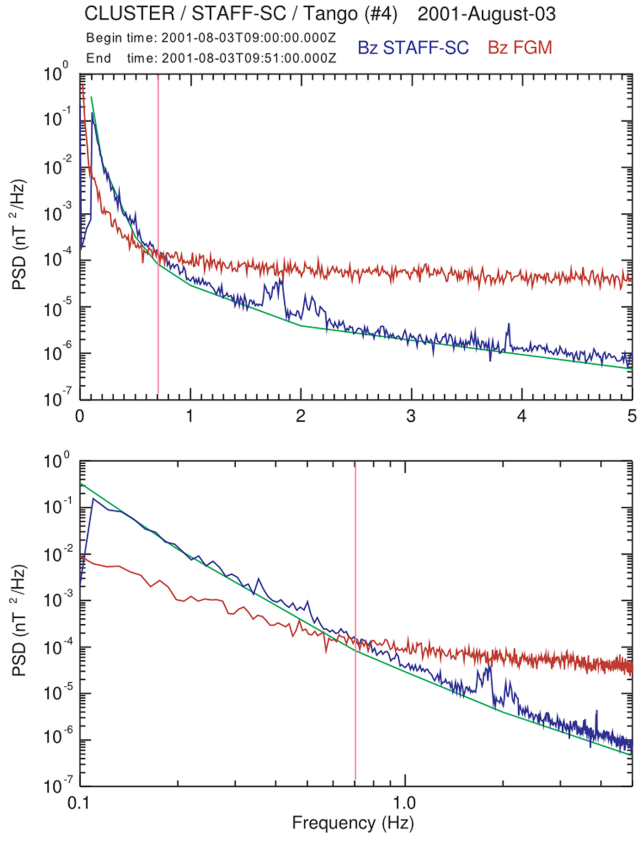

Figure 24. STAFF-FGM spectra comparison for a very low power event, to show respective sensitivity of the two instruments. Blue: STAFF, red: FGM. Top panel: lin–log scale, bottom panel: log–log scale. The green line is the STAFF ground measurement sensitivity, measured before launch, and corresponds roughly to the sensitivity observed in flight.

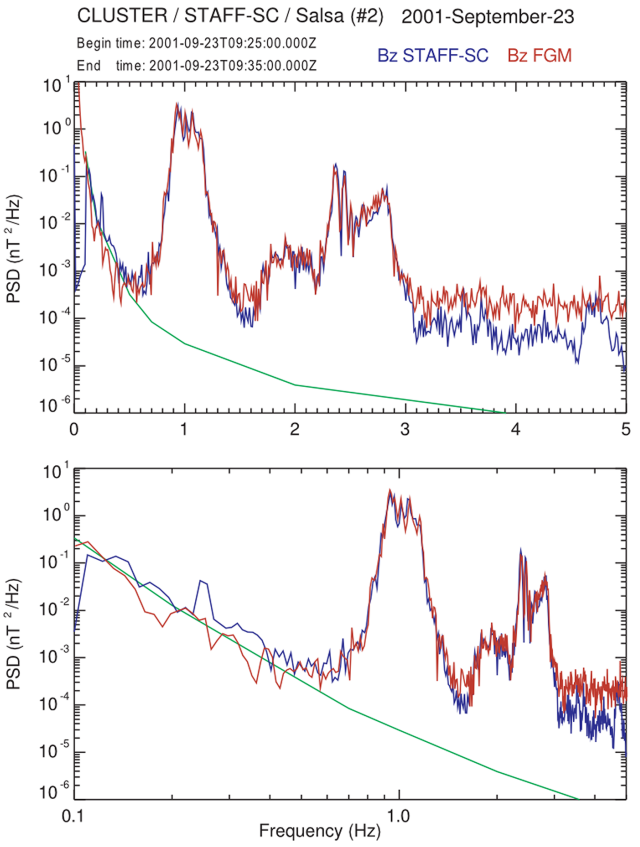

Figure 25. STAFF-FGM spectra comparison for events at 1 Hz.

low frequency below 0.4 Hz is not recorded by STAFF. This example is also a good illustration of the respective interest of the two instruments.

9.4.4 Wide frequency band event

Figure 27 shows a strong signal over the whole frequency bandwidth. The agreement is very good between 0.1 and $\sim$ 4 Hz. Above 4 Hz, the power spectral density ($nT^2\,Hz^{-1}$) of STAFF and FGM differs by a factor of nearly 2. Since the event is strong, the two instruments are widely above their sensitivity (the green line corresponds to the STAFF-SC sensitivity). Furthermore, this is STAFF, which is above FGM. A deeper study must be done to explain this. The effect of fall-off on the FGM frequency response at this frequency could be studied in a future work.

Figure 28 (from Nikiri et al., 2006) shows another example of power spectra comparison, in the cusp region. One can notice good agreement in the overlapping frequency bands, between 0.5 and 2 Hz, as for the previous 1 Hz event, so it confirms that below $\sim$ 4 Hz, the agreement is very good. It shows in the complementarity of both experiments, permitting analyses of a wide frequency range with good precision.

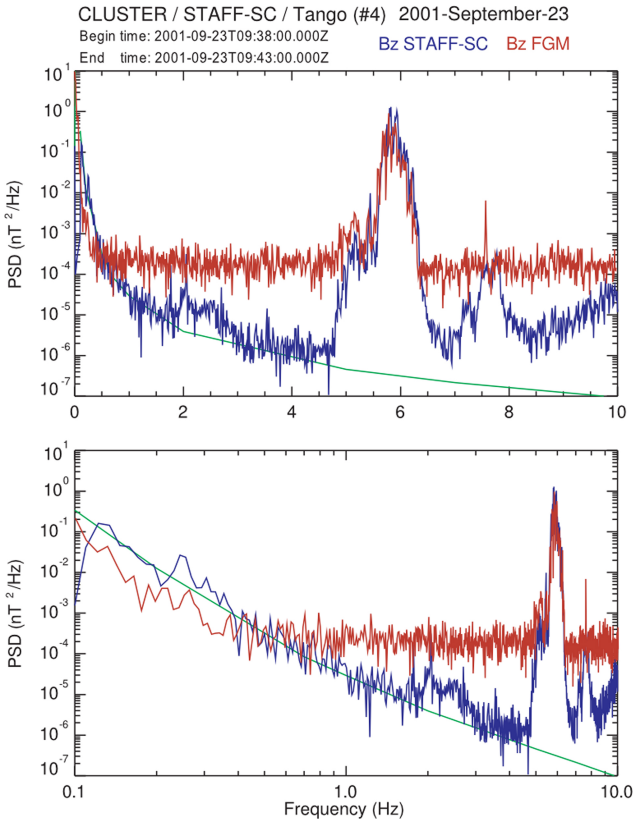

Figure 26. STAFF-FGM spectra comparison for events at 6 Hz.

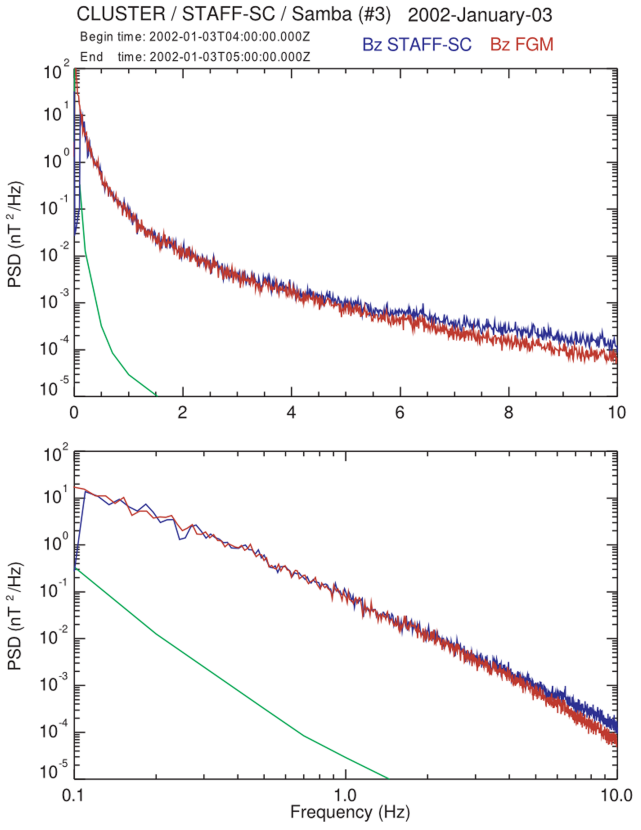

Figure 27. STAFF-FGM spectra comparison for a large frequency band event.

9.4.5 Doppler effect on sensitivity

Classical spectra are computed in the fixed (not spinning) system, as shown in Fig. 29, where we chose an event corresponding to the background noise. Ground sensitivity is plotted in black. Only the Z component (blue curve) is not disturbed by the spin, but the X and Y components (red and green curves respectively), in the spin plane, suffer from the Doppler effect: the large peak at spin frequency (0.25 Hz) corresponds to the 0 Hz frequency in the spinning system of the sensor, and thus could lead to an infinite value, since the transfer function at this frequency is null. Practically, to avoid an undefined value, one chooses a very low value rather than 0.

The two holes on X and Y at 0.25 ± 0.1 Hz correspond to the cut-off frequency chosen during the calibration (see Sect. 6). Furthermore, the spin effect added to the Doppler effect leads to a decrease in sensitivity in the X and Y components.

In other words, because the transfer function is close to zero at $f = 0$, this means that a right-handed polarised wave at spin frequency in the spinning coordinate system *cannot be recorded* by the STAFF sensor (see Fig. 30). Indeed, it is seen at $f = 0$ by the sensor, so the search coils do not provide any signal at this frequency. For this right wave,

$$f_{SR} = f_{SR2} - f_{spin}.$$

On the other hand, a left-handed polarised wave at any frequency, including DC, *is recorded* by the STAFF sensor. For this left wave,

$$f_{SR} = f_{SR2} + f_{spin}.$$

This also means that, at a low frequency, we *cannot* expect full agreement between STAFF and FGM, except for left-handed polarised waves, but for frequencies $f \gg f_{spin}$, as we found previously, there is good agreement.

To understand the consequences of the Doppler effect with a non-linear transfer function well, Fig. 31 shows this spectrum in the SR spinning coordinate. The peak at the spin frequency now corresponds to the DC magnetic field, and the cut-off frequency looks the same for the 3 XYZ components. Moreover, we can see that beyond twice spin frequency, the sensitivity becomes the same on the three components, which is not the case in the fixed SR2 system.

For more details on the Doppler effect on detected waves, see Robert et al. (1978, 1979) and Robert (1979a).

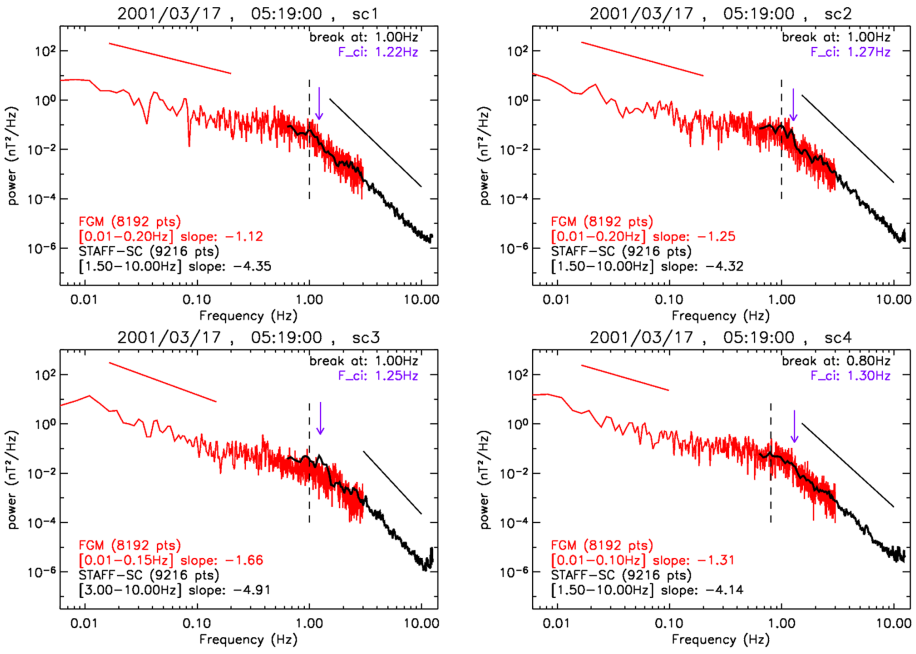

Figure 28. An example of comparison between FGM (in red) and STAFF (in black) power spectra, from Nikiri et al. (2006), in the cusp region. One can notice the good agreement in the overlap frequency bands, between 0.5 and 2 Hz. It shows that one can use a combination of the two complementary experiments, for instance to calculate the spectral power law index and the frequency break.

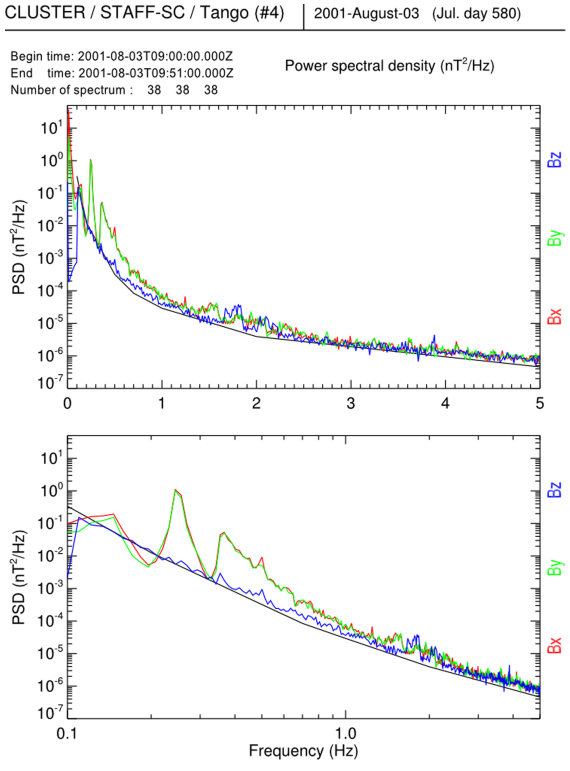

Figure 29. STAFF Power spectral density of background noise in the SR2 system.

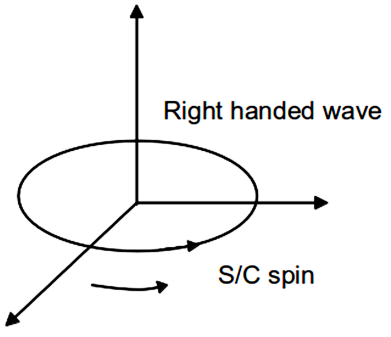

Figure 30. Schematic diagram illustrating the Doppler effect on the recorded waves.

10 Conclusions

A method to calibrate the waveform delivered by a rotating search coil has been proposed, and used for CLUSTER–STAFF-SC data. It has been shown that the solution to waveform calibration data is not unique and depends on the signal itself. Various coordinate systems required to transform telemetry data into a fixed and known coordinate system have been defined. The method and coordinate systems defined here can be used for another mission of the same kind. This paper also shows that the quality of the transfer functions of the instrument is a key to getting the best accurate calibrated waveforms and spectra. Sampling and transfer function determine the sensitivity of the instrument, which has

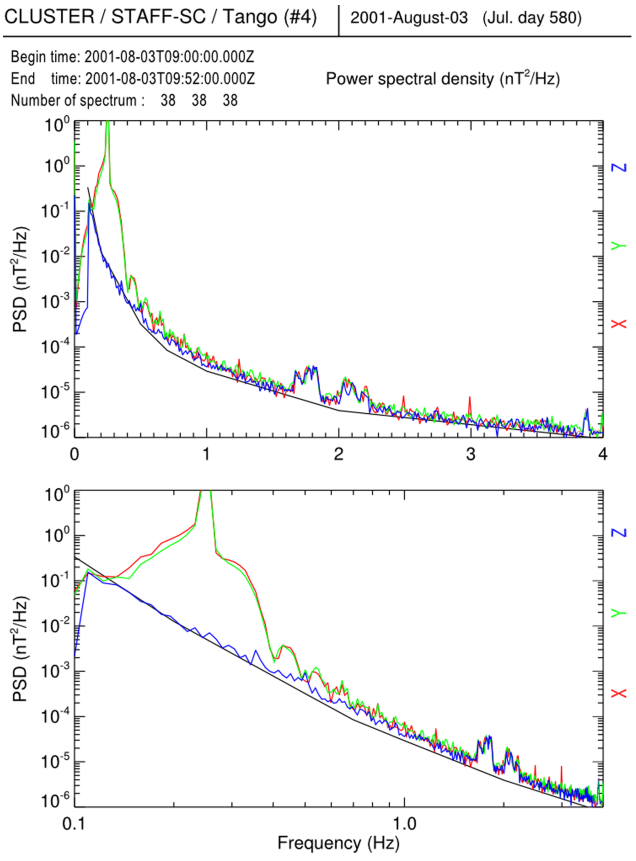

Figure 31. STAFF Power spectral density of background noise in the spinning system.

been established both from the calibrated waveform issued from STAFF-SC and for the calibrated spectra issued from STAFF-SA. It has been shown that we get good continuity between the two sub-instruments, into their common frequency range.

Cross-calibration between STAFF-SC in normal mode (0–10 Hz) and FGM in the same frequency range leads to an agreement of $\sim \pm 1$ % on the DC field in the spin plane and within a few % between 0.5 and 10 Hz. The respective sensitivity of the two instruments, deduced from observations done during a period of a very quiet magnetic activity, shows the two curves crossing at 0.7 Hz. Below this frequency, the fluxgate is more sensitive and gives the three components of the DC field. Above this frequency, the search coil is more sensitive.

Statistical study of the DC field, as measured by FGM and by STAFF at spin frequency over ten years, shows a constant difference between the two instruments, and so demonstrates the stability of the quality of measurements performed by both instruments.

Acknowledgements. The authors deeply thank A. Balogh, first PI of the FGM experiment, and the following ones, E. A. Lucek and C. Carr, and the whole FGM team, who contributed to delivering to the CAA an invaluable set of data available to the scientific community.

All engineers who have been working on the STAFF data since the beginning of the mission, too numerous to be mentioned, are fully thanked. The authors are indebted to Christophe Coillot for the establishment of the corrective transfer function formula, Bertrand de la Porte for the test on the transfer function, and Kateryna Musatenko for processing the in-flight calibration data.

Many thanks to the CAA itself for its action, and for the organisation of a long series of cross-calibration meetings from which a large part of this work is issued.

STAFF instrumentation and parts of data analysis have got support from ESA and CNES.

Edited by: H. Laakso

References

Balogh, A., Dunlop, M. W., Cowley, S. W. H., Southwood, D. J., Thomlinson, J. G., Glassmeier, K. H., Musmann, G., Lühr, H., Buchert, S., Acuña, M. H., Fairfield, D. H., Slavin, J. A., Riedler, W., Schwingenschuh, K., and Kivelson, M. G.: The cluster magnetic field investigation, Space Sci. Rev., 79, 65–91, 1997.

Balogh, A., Carr, C. M., Acuña, M. H., Dunlop, M. W., Beek, T. J., Brown, P., Fornacon, K.-H., Georgescu, E., Glassmeier, K.-H., Harris, J., Musmann, G., Oddy, T., and Schwingenschuh, K.: The Cluster Magnetic Field Investigation: overview of in-flight performance and initial results, Ann. Geophys., 19, 1207–1217, doi:10.5194/angeo-19-1207-2001, 2001.

Cornilleau-Wehrlin, N., Chauveau, P., Louis, S., Meyer, A., Nappa, J. M., Perraut, S., Rezeau, L., Robert, P., Roux, A., de Villedary, C., de Conchy, Y., Friel, L., Harvey, C. C., Hubert, D., Lacombe, C., Manning, R., Wouters, F., Lefeuvre, F., Parrot, M., Pinçon, J. L., Poirier, B., Kofman, W., and Louarn, P.: The CLUSTER Spatio-Temporal Analysis of Field Fluctuations (STAFF) Experiment, Space Sci. Rev., 79, 107–136, 1997.

Cornilleau-Wehrlin, N., Chanteur, G., Perraut, S., Rezeau, L., Robert, P., Roux, A., de Villedary, C., Canu, P., Maksimovic, M., de Conchy, Y., Hubert, D., Lacombe, C., Lefeuvre, F., Parrot, M., Pinçon, J. L., Décréau, P. M. E., Harvey, C. C., Louarn, Ph., Santolik, O., Alleyne, H. St. C., Roth, M., Chust, T., Le Contel, O., and STAFF team: First results obtained by the Cluster STAFF experiment, Ann. Geophys., 21, 437–456, doi:10.5194/angeo-21-437-2003, 2003.

Cross Calibration Workshops: The purpose of the cross-calibration workshops is to provide a forum where observations from different Cluster instruments are compared in detail, presentations of organized workshops between September 2005 and March 2013, available at: ftp://ftp.lpp.polytechnique.fr/robert/keep/Biblio_et_CV/ESA_CrossCal_Meetings, 1st CrossCal Workshop, ESTEC, 2–3 February2006/CrossCal01-STAFF_Robert.ppt, 2nd CrossCal Workshop, ESTEC, 16 May 2006/CrossCal02-STAFF_Robert.ppt, 8th CrossCal Workshop, Kinsale, Co. Cork, Ireland, 28–30 October 2008/CrossCal08-STAFF_Robert.ppt 9th CrossCal Workshop, Jesus College, Cambridge, 23–27 March 2009/CrossCal09-STAFF_Burlaud.ppt, 10th CrossCal

Workshop, L'Observatoire de Paris, Paris, 3–4 November 2009/CrossCal10-STAFFActions_Burlaud.ppt/CrossCal10-STAFF-SA_De_Conchy.ppt/CrossCal10-STAFF-SC_Robert.ppt, 11th CrossCal Workshop, Hotel die Tanne, Goslar, 7–9 April 2010/CrossCal11-STAFF_Burlaud.ppt,/CrossCal11-STAFF_Robert.ppt, 12th CrossCal Workshop, CESR, Toulouse, 26–28 October 2010/CrossCal12-STAFF_Cornilleau.ppt, /CrossCal11-STAFF_Robert.ppt, 13th CrossCal Workshop, IRF, Uppsala, Sweden, 13–15 April 2011/CrossCal13-STAFF_Robert.ppt, 14th CrossCal Workshop, York, UK, 5–7 October 2011/CrossCal14-STAFF_Robert.ppt/CrossCal14-STAFF_Santolik.ppt, 15th CrossCal Workshop, University College of London, London, 17–19 April 2012/CrossCal15-STAFF_Robert_Piberne.pptx, 16th CrossCal Workshop, Toulouse, France, 6–9 November 2012/CrossCal16-STAFF_Robert_Piberne.ppt, 17th CrossCal Workshop, ESOC, Darmstadt, Germany, 25–27 March 2013/CrossCal17-STAFF_Piberne.ppt, 18th CrossCal Workshop, Cosener's House, Abingdon, UK, 23–25 October 2013/CrossCal18-STAFF_Piberne.pptx.

Gurnett, D. A., Huff, R. L., and Kirchner, D. L.: The wide-band plasma wave investigation, Space Sci. Rev., 79, 195–208, 1997.

Gustafsson, G., Boström, R., Holback, B., Holmgren, G., Lundgren, A., Stasiewicz, K., Ahlén, L., Mozer, F. S., Pankow, D., Harvey, P., Berg, P., Ulrich, R., Pedersen, A., Schmidt, R., Butler, A., Fransen, A. W. C., Klinge, D., Thomsen, M., Fälthammar, C. G., Lindqvist, P.-A., Christenson, S., Holtet, J., Lybekk, B., Sten, T. A., Tanskanen, P., Lappalainen, K., and Wygant, J.: The electric field and wave experiment for the Cluster mission, Space Sci. Rev., 79, 137–156, 1997.

Harvey, C. C., Belkacemi, M., Manning, R., Wouters, F., de Conchy, Y.: STAFF Spectrum Analyzer, Conversion of the Science Data to Physical Units, Technical Report OBSPM-0001, issue 7, rev. 5, Observatoire de Paris Meudon, Paris, 2004.

Jones, D.: Introduction to the S-300 wave experiment onboard GEOS, Space Sci. Rev., 22, 327–332, 1977.

Knott, K.: Payload of the GEOS scientific geostationary satellite, ESA Sci. Tech. Rev., 1, 173–196, 1975.

Le Contel, O., Roux, A., Robert, P., Coillot, C., Bouabdellah, A., de la Porte, B., Alison, D., Ruocco, S., Angelopoulos, V., Bromund, K., Chaston, C. C., Cully, C., Auster, H. U., Glassmeier, K. H., Baumjohann, W., Carlson, C. W., McFadden, J. P., and Larson, D.: First results of the THEMIS Search Coil Magnetometers, Space Sci. Rev., 141, 509–534, doi:10.1007/s11214-008-9371-y, 2008.

Nykyri, K., Grison, B., Cargill, P. J., Lavraud, B., Lucek, E., Dandouras, I., Balogh, A., Cornilleau-Wehrlin, N., and Rème, H.: Origin of the turbulent spectra in the high-altitude cusp: Cluster spacecraft observations, Ann. Geophys., 24, 1057–1075, doi:10.5194/angeo-24-1057-2006, 2006.

Paschmann, G., Melzner, F., Frenzel, R., Vaith, H., Parigger, P., Pagel, U., Bauer, O. H., Haerendel, G., Baumjohann, W., Sckopke, N., Torbert, R. B., Briggs, B., Chan, J., Lynch, K., Morey, K., Quinn, J. M., Simpson, D., Young, C., McIllwain, C. E., Fillius, W., Kerr, S. S., Mahieu, R., and Whipple, E. C.: The electron drift instrument for cluster, Space Sci. Rev., 79, 233–269, 1997.

Pedersen, A., Cornilleau-Wehrlin, N., de la Porte, B., Roux, A., Bouabdellah, A., Décréau, P. M. E., Lefeuvre, F., Sené, F. X., Gurnett, D., Huff, R. R., Gustafsson, G., Holmgren, G., Woolliscroft, L. J. C., Thompson, J. A., and Davies, P. H. N.: The Wave Experiment Consortium (WEC), Space Sci. Rev., 79, 93–106, 1997.

Perry, C., Eriksson, T., Escoubet, P., Esson, S., Laakso, H., McCaffrey, S., Sanderson, T., and Bowen, H.: The ESA Cluster Active Archive, in: Proceedings of the Cluster and Double Star Symposium 5th Anniversary of Cluster in Space, ESTEC, Noordwijk, 2005.

Pinçon, J. L. and Lefeuvre, F.: Local characterization of homogeneous turbulence in a space plasma from simultaneous measurements of field components at several points in space, J. Geophys. Res., 96, 1789–1802, 1991.

Robert, P.: Cluster software tools – Part I: Coordinate transformations library, Document de Travail, DT/CRPE/1231, July, available at: ftp://ftp.lpp.polytechnique.fr/robert/keep/Biblio_et_CV/Working_documents/1993_Robert_DTCRPE1231_ROCOTLIB.pdf (last access: 3 December 2013), 1993.

Robert, P.: Intensité et polarisation des ondes UBF détectées à bord de GEOS-1, Méthode d'analyse numérique du signal et production en routine de sommaires expérimentateurs, Problèmes rencontres et solutions pratiques, Note Technique CRPE/ETE/71, May, available at: ftp://ftp.lpp.polytechnique.fr/robert/keep/Biblio_et_CV/Working_documents/1979_Robert_NTCRPE71_Intensite_et_Polarisation_des_ondes_UBF.pdf (last access: 4 December 2013), 1979a.

Robert, P.: Measurement by the S-300 experiment of two components of the DC magnetic field, in the X–Y plane of the satellites GEOS-1 and GEOS-2, Comparison with the results of the S-331 magnetometer, Document de Travail CRPE/ETE, July, available at: ftp://ftp.lpp.polytechnique.fr/robert/keep/Biblio_et_CV/Working_documents/1979_Robert_DTCRPE_Measurement_by_S300_of_2comp_DC_field.pdf (last access: 3 December 2013), 1979b.

Robert, P.: ROCOTLIB: a rather complete suite of coordinate transformation routines, Issue 1, Rev. 8, November 2003, available at: http://cdpp.eu/index.php/Scientific-libraries/rocotlib.html (last access: 3 December 2013), 2003.

Robert, P.: ROCOTLIB: a coordinate Transformation Library for Solar-Terrestrial studies, & french version, ROCOTLIB: une bibliothèque de changement de coordonnées pour les études Soleil-Terre Le Bulletin du Centre de Données de la Physique des Plasmas Num. 8t, CNES, 2004.

Roberg, P.: Cross Calibration Workshops, document "CrossCal10-STAFFSC_Robert.ppt", L'Observatoire de Paris, 3–4 November 2009, Paris, 2009.

Robert, P., Kodera, K., Perraut, S., Gendrin, R., and de Villedary, C.: Polarization characteristics of ULF waves detected onboard GEOS-1, Problems encountered and practical solutions, XIXth URSI General Assembly, Helsinki, Finland, 31 July–8 August, available at: ftp://ftp.lpp.polytechnique.fr/robert/keep/Biblio_et_CV/Publications/1978_Robert_URSI_Helsinki.pdf (last access: 3 December 2013), 1978.

Robert, P., Kodera, K., Perraut, S., Gendrin, R., and de Villedary, C.: Amplitude et polarisation des ondes UBF détectées à bord du satellite GEOS-1, Méthodes d'analyse, problèmes rencontrés et solutions pratiques , Ann. Télécommun., 34, 179–186, 1979.

Robert, P., Burlaud, C., Maksimovic, M., Cornilleau-Wehrlin, N., and Piberne, R.: Calibration Report of the STAFF Measurements in the Cluster Active Archive (CAA), Doc. No. CAA-STA-CR-002, issue 3.0, 16 May 2012, available at: http://caa.estec.esa.int/documents/CR/CAA_EST_CR_STA_v30.pdf (last access: 3 December 2013), 2012.

Roux, A., Le Contel, O., Robert, P., Coillot, C., Bouabdellah, A., de la Porte, B., Alison, D., Ruocco, S., and Vassal, M. C.: The search coil magnetometer for THEMIS, Space Sci. Rev., 141, 265–275, doi:10.1007/s11214-008-9455-8, 2008.

Santolik, O.: Propagation Analysis of STAFF-SA Data with Coherency Tests (a User's Guide to PRASSADCO), LPCE/NTS/073.D, Lab. Phys. Chimie Environ./CNRS, Orleans, France, available at: http://aurora2.troja.mff.cuni.cz/~santolik/PRASSADCO/tc2/doc/guide.pdf (last access: 3 December 2013), 2003.

Santolik, O., Parrot, M., and Lefeuvre, F.: Singular value decomposition methods for wave propagation analysis, Radio Sci., 38, 1010, doi:10.1029/2000RS002523, 2003.

Woolliscroft, L. J. C., Alleyne, H. S. C., Dunford, C. M., Sumner, A., Thompson, J. A., Walker, S. N., Yearby, K. H., Buckley, A., Chapman, S., Gough, M. P., and the DWP Coinvestigators: The digital wave processing experiment on Cluster, Space Sci. Rev., 79, 209–231, 1997.